A DNM2 centronuclear myopathy mutation reveals a link between recycling endosome scission and autophagy

Claudia Puri[1,2,3], Marco M. Manni[1,2], Mariella Vicinanza[1,2,3], Christine Hilcenko[2,4,5], Ye Zhu[1,2], Gautam Runwal[1,2], Eleanna Stamatakou[1,2,3], Fiona M. Menzies[1,2], Kamel Mamchaoui[6], Marc Bitoun[6], and David C. Rubinsztein[1,2,3]*~

[1]Department of Medical Genetics Cambridge Biomedical Campus, Hills Road, Cambridge CB2 0XY, UK, [2]Cambridge Institute for Medical Research Cambridge Biomedical Campus, Hills Road, Cambridge CB2 0XY, UK, [3]UK Dementia Research Institute, The Keith Peters Building Cambridge, Cambridge Biomedical Campus, Hills Road, Cambridge CB2 0XY, UK, [4] Department of Haematology, University of Cambridge, Cambridge, CB2 0XY, UK,[5] Wellcome Trust–Medical Research Council Stem Cell Institute, University of Cambridge, Jeffrey Cheah Biomedical Centre Puddicombe Way Cambridge Biomedical Campus Cambridge CB2 0AW [6]Myology Center for Research, U974, Sorbonne Université - INSERM - AIM, GH Pitie Salpetrière, F-75013, Paris, France

~ Lead Contact: dcr1000@cam.ac.uk

* email address of corresponding author: dcr1000@cam.ac.uk

SUMMARY

Autophagy involves engulfment of cytoplasmic contents by double-membraned autophagosomes, which ultimately fuse with lysosomes to enable degradation of their substrates. We recently proposed that the tubular-vesicular recycling endosome membranes was a core platform on which the critical early events of autophagosome formation occurred, including LC3-membrane conjugation to autophagic precursors. Here we report that the release of autophagosome precursors from recycling endosomes is mediated by DNM2-dependent scission of these tubules. This process is regulated by DNM2 binding to LC3, and is increased by autophagy-inducing stimuli. This scission is defective in cells expressing a centronuclear myopathy-causing DNM2 mutant. This mutant has an unusual mechanism as it depletes normal-functioning DNM2 from autophagosome formation sites on recycling endosomes by causing increased binding to an alternative plasma membrane partner, ITSN1. This "scission" step is thus critical for autophagosome formation, is defective in a human disease, and influences the way we consider how autophagosomes are formed.

KEYWORDS: Autophagy; recycling endosome; DNM2; ITSN1; centronuclear myopathy.

INTRODUCTION

Macroautophagy (henceforth autophagy) is the process where cells engulf cytoplasmic contents in double-membraned autophagosomes, which traffic their contents to lysosomes for degradation (Fass et al., 2006). This pathway, which is conserved from yeast to humans, helps maintain cellular homeostasis by degrading substrates like protein complexes, aggregate-prone proteins (e.g. in neurodegenerative diseases), various pathogens, and dysfunctional organelles (like mitochondria and peroxisomes) (Eskelinen, 2019; Menzies et al., 2017). Accordingly, autophagy impacts many human diseases, including forms of neurodegeneration, cancer, infections and inflammation (Hansen et al., 2018; Tang et al., 2019).

A key question is how do cells generate these vesicles that have double membranes? The precursors of autophagosomes are cup-shaped double-membrane structures called phagophores. These originate from membranes where key events occur, including PI(3)P (phosphatidylinositol 3-phosphate) synthesis mediated by an enzyme complex including Beclin 1 and the PI 3-kinase VPS34, which leads to the PI(3)P-dependent recruitment of WIPI2, which then recruits the ATG5-12/ATG16L1 complex that enables the conjugation of ATG8 family members (like LC3s) to the nascent phagophore membranes. This ubiquitin-like conjugation of ATG8 members to autophagosomes represents a defining step in autophagosome formation (Dooley et al., 2014; Vicinanza et al., 2015).

Many different membranes have been proposed to contribute to autophagosomes including the plasma membrane, endosomes, various domains of the ER (endoplasmic reticulum) and the Golgi apparatus (Axe et al., 2008; Hamasaki et al., 2013; Hayashi-Nishino et al., 2009; Knaevelsrud et al., 2013a; Longatti et al., 2012; Puri et al., 2013; Puri et al., 2018a; Ravikumar et al., 2010; Shibutani and Yoshimori, 2014; Yla-Anttila et al., 2009). We recently proposed that the recycling endosome RAB11A-positive membranes were a core platform on which the critical early events of autophagosome formation occurred leading up to LC3 conjugation - the recruitment of WIPI2 and subsequent autophagosome formation was not only dependent on PI(3)P (which is also found in membranes that are known not to direct form

autophagosomes) but also required WIPI2 binding to RAB11A (Puri et al., 2018a). Our previous data suggested that most, if not all, autophagosomes had this RAB11A-dependency for their formation – for instance, WIPI2 knockdown cells reconstituted with mutant forms of WIPI2 that could not bind RAB11A had almost complete abrogation of WIPI2- or ATG16L1-positive autophagosome precursors, compared to those reconstituted with wild-type WIPI2 (Puri et al., 2018a). Furthermore, WIPI2 knockdown cells reconstituted with mutant forms of WIPI2 that could not bind RAB11A had increased levels of autophagy substrate accumulation (mutant huntingtin aggregation) similar to WIPI2 knockdown cells, while those cells reconstituted with wild-type WIPI2 had much lower levels (~ 50%) of these substrates, similar to control cells. The RAB11A structures that acquired LC3 were considered to be autophagosomes as they had double membranes, and engulfed autophagic substrates like p62, mutant huntingtin and mitochondria (Puri et al., 2018a). Our data are compatible with other recent studies that link autophagy and the recycling endosome (Izumi et al., 2019; Longatti et al., 2012; Puri et al., 2013; Soreng et al., 2018).

If the key molecular events leading to and including LC3 conjugation to nascent autophagosome membranes occur on tubular-vesicular recycling endosome membranes, this can explain how autophagosomes have double membranes and why endocytosed transferrin and the extracellular domain of the transferrin receptor are found between the inner and outer membranes of phagophores/autophagosomes (Longatti et al., 2012; Puri et al., 2018a). This phenomenon is consistent with the membrane topology that would arise if the two membranes of autophagosomes formed from recycling endosome tubules (Puri et al., 2018b). However, this model requires a step of recycling endosome tubule scission to release nascent phagophores, a step in autophagosome formation which has previously not been described.

An important mediator of tubulated membrane scission in other cellular contexts is dynamin 2 (DNM2), a ubiquitously expressed large GTPase (Ferguson and De Camilli, 2012). DNM2 comprises five domains: an N-terminal GTPase domain, followed by the middle and pleckstrin homology (PH) domains, the GTPase effector domain (GED), and the C-terminal proline/arginine-rich domain (PRD). DNM2 mutations cause autosomal dominant centronuclear myopathy, a condition that

manifests with muscle weakness and wasting (Hohendahl et al., 2016; Zhao et al., 2018). Mutations affecting the middle domain (MD) are generally associated with a relatively mild clinical course, while those in the pleckstrin-homology (PH) and GTPase effector (GED) domains are more severe (Catteruccia et al., 2013). One of the best characterized CNM mutations in DNM2 is R465W in the middle domain (Buono et al., 2018; Durieux et al., 2012; Durieux et al., 2010). Fibroblasts from DNM2 R645W heterozygous (HTZ) mice have defective autophagy with an accumulation of immature autophagic structures (Durieux et al., 2012). Our data explain this phenotype, reveal a new step where autophagy can be blocked in disease and characterize the mechanism, since the DNM2 R465W mutation reveals an unforeseen link between recycling endosome scission and autophagy.

RESULTS

Recycling endosomes fragment to release nascent autophagosomes

When autophagy is induced with mTOR-dependent or –independent stimuli, the recycling endosome RAB11A-positive tubules fragment and LC3-positive structures are released from this compartment (Fig.1A-C and Movie 1). We tested if DNM2 (dynamin 2) mediated this process, as cells with the DNM2 R465W mutation that causes autosomal dominant centronuclear myopathy manifest an accumulation of immature autophagic structures (Durieux et al., 2012). DNM2 detaches endocytic vesicles from the plasma membrane (Ferguson and De Camilli, 2012; Sundborger and Hinshaw, 2014) but is also present on recycling endosomes (Soreng et al., 2018; van Dam and Stoorvogel, 2002). We isolated recycling endosomes by magnetic isolation after chasing iron microbeads conjugated to the transferrin-Alexa Fluor 488 into this compartment (Puri et al., 2018a). Using this approach, we confirmed the presence of DNM2 on recycling endosomes along with RAB11A and LC3 (Fig. S1A). Interestingly the DNM2 plasma membrane binding partner, ITSN1 (Intersectin-1), was not seen in the recycling endosomes fraction but only on the "unbound" fraction (Fig. S1A). DNM2 co-localised with RAB11A in LC3-positive structures by confocal and superresolution structured illumination (SIM) microscopy (Fig. 1D-E). Live imaging suggested that LC3 is present on the RAB11A compartment before DNM2, which appears to localize at the junction of LC3 and RAB11A (Fig. 1F). Later in the movie, DNM2 looked like it enwrapped both LC3 and RAB11A-labelled structures before autophagosome release from the recycling endosome (Fig. 1F, Fig. S1B and Movie 2).

LC3 directly interacts with DNM2

LC3 becomes LC3-II, which has a characteristic gel mobility, after it is conjugated to autophagic precursor membranes (Kabeya et al., 2000). DNM2 RNAi silencing led to LC3-II accumulation in nutrient replete (Fig. 2A and S2A) or in starvation (Fig. S2B) conditions but not when cells were treated with the lysosomal inhibitor, Bafilomycin A1, which blocks LC3-II/autophagosome degradation, suggesting that DNM2 regulates a step in autophagy downstream of LC3 conjugation to nascent autophagosome membranes. DNM2 knockdown also caused an increase of cells with RAB11A tubules (Fig. 2B), which would result from impaired recycling endosome fragmentation, and increased colocalisation of LC3-positive structures with the

RAB11A compartment (Fig. 2C-D). These data support a role for DNM2 in recycling endosome fragmentation to enable the release of LC3-positive structures (phagophores/autophagosomes).

We considered that DNM2 binding to recycling endosomes may be LC3-dependent. Endogenous LC3 (Fig. S2C) or GFP-tagged exogenous LC3 can bind DNM2 and the binding increases when the cells are treated with different autophagy inducers (starvation-HBSS, rapamycin and SMER28) (Fig. 2E-F and S2C). As in vitro experiments confirmed that the LC3-DNM2 interaction was direct (Fig. 2G), we searched for a potential LC3-interacting region (LIR) motif in DNM2 (Fig. 2H). Mutagenesis experiments suggested that amino acids 523-528 were critical, as mutation of tryptophan 525 abolished the DNM2-LC3 interaction (Fig. 2I). The protein carrying this mutation is still functional, since it still binds its plasma membrane interactor ITSN1 (Fig. S2D). DNM2 knockdown cells were reconstituted with either wild-type or LIR-mutant (W525L) DNM2 and we observed that the LIR-mutant-expressing cells had a phenotype similar to what we observed in DNM2-depleted cells (Fig. 2A-D): an increase of cells with RAB11A tubules, an increased colocalisation of LC3-positive structures with the RAB11A compartment, decreased DNM2 colocalisation with RAB11A (Fig. 2J), and LC3-II accumulation in nutrient replete (Fig. 2K) or starvation conditions (Fig. S2E) in the absence but not in the presence of Bafilomycin A1. DNM2 WT re-expression in DNM2-depleted cells normalized the LC3 elevation caused by DNM2 depletion, which was not seen with the DNM2 W525L mutant (Fig. S2F). Interestingly, stable overexpression of this DNM2-LIR mutant without knockdown in starved cells phenocopied the LC3-II elevation in the absence of Bafilomycin and no change in the presence of Bafilomycin seen in DNM2-knockdown cells reconstituted with the mutant (Fig. S2E and S2G). Thus, this mutant likely acts as a dominant-negative, as DNM2 works as an oligomer (Ross et al., 2011).

We modelled the DNM2-LC3 interaction using PyMOL software (http://www.pymol.org) (Fig. 2L) to find the LC3 domain important for DNM2 interaction. We tested mutations in two different amino acids, K51 and R70 that help form a putative DNM2-binding pocket. K51 is known to be responsible for the

autophagy adaptor SQSTM1/P62 interaction (Chino et al., 2019; Tung et al., 2010). The LC3 K51A mutation affects LC3 interactions with both P62 and DNM2, but LC3 R70A affects only the LC3-DNM2 interaction (Fig. 2M).

Consistent with our hypothesis that LC3 recruits DNM2 to the recycling endosome to enable scission and LC3/autophagosome release, the LC3 R70A mutant localized more on RAB11A compartment compared with the WT, and the LC3 R70A dots on RAB11A did not associate with DNM2, while the WT LC3 clearly associated with DNM2 (Fig. S3A). K51 and R70 are conserved in other ATG8 family members (Fig. S3B) and DNM2 also binds other ATG8 members, like GABARAP, GABARAP-L1 and GABARAP-L2 (Fig. S3B-C).

LC3 conjugation to phosphatidylethanolamine to form LC3-II is completed by the E2-like enzyme ATG3 and then the E3-like ATG16L1-ATG5-ATG12 complex (Gao et al., 2013). Since DNM2 can still bind LC3 in ATG3-null cells, DNM2 can bind non-lipidated LC3 (Fig. S3D). (P62 can also bind non-lipidated LC3 (Fig. S3D)).

DNM2 is GTPase protein. GTPase proteins cycle between the cytosol (by binding GDIs, GDP dissociation inhibitors) and the membrane, and when on membranes cycle between inactive (GDP-bound) and active (GTP-bound) states. This enables specificity of membrane localization of GTPases. This means that most interactions GTPases are transient and it is not surprising that they appear to be low (Antonny et al., 2016). Furthermore, DNM2 acts in a number of sites in the cell and thus it is not exclusively associated with a single partner.

Cells expressing DNM2 R465W accumulate autophagosomes on recycling endosome

The DNM2 R465W centronuclear myopathy mutation causes an accumulation of immature autophagosomes (Durieux et al., 2012), which we confirmed both in patient fibroblasts (with endogenous protein) and in HeLa cells (with stably overexpressed wild-type or R465W DNM2), where we found that cells expressing R465W contained mainly phagophores and autophagosomes and very few autolysosomes, in contrast with wild-type cells that had mostly autolysosomal structures (Fig. 3A-B). Mutant huntingtin exon 1 is a well-validated autophagy substrate and the proportions of cells with aggregates correlate directly with the levels of the protein, all other factors being

equal (Narain et al., 1999). Overexpression of DNM2 R465W mutant increased the percentages of cells with aggregates of mutant huntingtin exon 1 (Q74 aggregates (Fig. 4A)). The R465W mutation is not in the LIR domain, yet binds much less LC3 in cells than the WT (Fig. 4B). Overexpression of the DNM2 R465W mutant phenocopied cells with the DNM2-LIR mutant (Fig. 2J) and caused an increase of the RAB11A tubules compared with overexpression of the WT (Fig. 4C and Fig. S4A), decreased colocalization of LC3 with DNM2 R465W, increased colocalisation of LC3 with RAB11A (Fig. 4C), decreased DNM2-RAB11A colocalisation (Fig. 4D) and increased LC3-II in nutrient replete (Fig. 4E) or starvation conditions but not with Bafilomycin A1 (Fig. S4B-C uses DNM2 knockdown cells reconstituted with either wild-type or R465W).

Cells expressing DNM2 mutants accumulate immature autophagosomes

DNM2 is an important component of the endocytic machinery. Importantly, endocytosis was normal in HeLa cells overexpressing DNM2 R465W (as it is also in the LIR mutant) and in cells where we used a 3 days knockdown protocol employed throughout this study, (which still leaves some residual DNM2) (Fig. S5A). Our results are consistent with previous data using DNM2 R465W heterozygous mouse embryonic fibroblasts (Ali et al., 2019; Durieux et al., 2010). We observed similar normal localization of ATG9A and ATG16L1 on RAB11A-positive structures (Puri et al., 2013) in cells expressing wild-type, R465W or W525L forms of DNM2, suggesting that these mutants do not affect the trafficking of these ATG proteins (Fig. 5A and S5B). We previously showed that ATG9A is trafficked from the plasma membrane to recycling endosomes (Puri et al., 2013). Using an antibody that we generated against the ATG9A II extracellular loop (validated in Fig S5C, we confirmed that the endocytosed ATG9A colocalised with LC3-positive structures (Fig. S5D). We conjugated this anti-ATG9A antibody with micromagnetic beads (FerroFluid) and allowed these conjugates to be endocytosed for 1 h and chase for 15 min (Puri et al., 2018a) into HeLa cells stably expressing wild-type, R465W or W525L DNM2. The membranes containing the anti-ATG9A-Ferrofluid beads were separated magnetically (bound) and compared with the rest of the lysate (unbound). We confirmed that ATG9A was present in the bound fraction (as it is a multipass transmembrane protein) and that the amount of ATG16L1 on the bound fraction was very similar in DNM2 WT cells and the two mutants (Fig. 5B and S5E), suggesting

that the ATG9A trafficking leading to colocalisation of ATG16L1 with ATG9A (Puri et al., 2013) was not affected by these DNM2 mutations. Moreover, both DNM2 mutants (W525L and R465W) were still able to bind SNX18 (sorting nexin 18) (Knaevelsrud et al., 2013b; Soreng et al., 2018) (Fig. S5F), and since we did not observe abnormal ATG9A trafficking with R465W or W525L DNM2 (Fig. 5A-B and S5B, E), we concluded that the DNM2-LC3 biology is likely distinct from any effects of SNX18 in ATG9A trafficking from recycling endosomes (Fig. S5F).

We thus tested if the DNM2 R465W and DNM2-LIR mutants (W525L) shared other autophagy phenotypes. We first transfected wild-type DNM2 or the two mutants in a HeLa stable cell line expressing the tandem tagged mRFP-GFP-LC3, which allows discrimination between non-acidified structures like autophagosomes/phagophores and acidified autolysosomes, since the former emit both RFP and GFP signals, whereas the acidic pH in lysosomes denatures GFP so that only RFP fluorescence is observed (Kimura et al., 2007). Both mutants caused a build-up of non-acidified structures at the expense of acidified structures, suggesting a block in autophagy upstream of autophagosome-lysosome fusion (Fig. 5C and S5G). We also used the HaloTag-LC3 autophagosome completion assay that specifically detects phagophores, nascent autophagosomes and mature autophagic structures by exploiting membrane-impermeable Alexa Fluor (AF) 488 HaloTag (MIL) and membrane-permeable tetramethylrhodamine HaloTag ligands (MPL) (Takahashi et al., 2018). This assay suggested that the mutants caused no change in the numbers of open phagophores, but led to an accumulation of autophagosomes and a reduction of autolysosomes, compatible with the mRFP-GFP-LC3 data above (Fig. 5D-E). This defect is unlikely due to lysosomal defects, since cathepsin D maturation (which is impaired by raised lysosomal pH and some other defects) was similar in cells expressing wild-type and mutant forms of DNM2 (Fig. 5F and S5H) or in DNM2 knockdown cells (Fig. S5I). Interestingly, in cells transfected with DNM2 R465W, LC3 vesicles were not able to detach from the RAB11A-positive compartment, moved along the tubules and accumulated at the perinuclear region of the compartment (Fig. S5J and K and Movie 3). Thus, our data suggest that this mutant regulates the release of nascent autophagosomes from RAB11A-positive recycling endosomes.

ITSN1 sequesters DNM2 R465W on plasma membrane

These data all suggest that overexpression of DNM2 R465W compromises autophagy and mimics the autophagic phenotypes resulting from DNM2 loss-of-function or loss-of-LC3 binding – impaired release of LC3 containing membranes from the RAB11A compartment due to reduced scission. We wanted to resolve why the DNM2 R465W (CNM) mutant is not able to bind LC3 when the mutation is not in the DNM2 LIR domain. A clue emerged when immuno-electron microscopy showed DNM2 R465W in plaques on the plasma membrane (Fig. 6A) and total internal reflection fluorescence (TIRF) microscopy revealed that DNM2 R465W localizes more with the clathrin adaptor AP2 on plasma membrane than the wild-type protein (Fig. 6B). On the plasma membrane, DNM2 interacts with intersectin 1 (ITSN1), a protein which acts as a scaffold for dynamin and other endocytic proteins ensuring its recruitment to sites of endocytosis (Sundborger and Hinshaw, 2014). Notably ITSN1 is not present on recycling endosomes (Fig. S1A). We found that DNM2 R465W bound more ITSN1 than the WT (Fig. 6C-D), which suggested that the DNM2 R465W mutant was not recruited to the site of autophagosome biogenesis (binds less LC3 (Fig. 4B)) because it is sequestered away from the recycling endosome to the plasma membrane by ITSN1. This model was supported when we observed that while cells expressing the DNM2 R465W mutant have more RAB11A tubules/less fragmentation (Fig. 4C), this phenotype was normalized when ITSN1 was depleted (Fig. 6E and S6A). In cells overexpressing DNM2 R645W, ITSN1 knockdown reduced the amount of DNM2 R465W at the plasma membrane (by TIRF microscopy, Fig. 6F and S6B-C), recruited DNM2 R465W back to the recycling endosome (by superresolution SIM microscopy, Fig. 6G), enabled DNM2 R465W-LC3 binding (Fig. 6H) and increased autophagosome formation (LC3 level in basal and under Bafilomycin A1 conditions (Fig. 6I-S6D)). By contrast, when we silenced ITSN1 in cells reconstituted with the DNM2 LIR mutant (W525L), we observed no effect on LC3 levels, supporting the idea that the defect of LC3 binding for the DNM2 LIR mutant is independent of ITSN1 binding (Fig. 6J). Thus, the DNM2 CNM R465W mutant, in contrast to the LIR mutant, is still able to bind LC3 efficiently and release of the autophagosomes from the recycling endosomes, but its mutation causes it to bind more to ITSN1, which diverts the CNM mutant to the plasma membrane to function in clathrin-mediated endocytosis, but away from recycling endosomes, thereby compromising release the nascent autophagosomes.

R465W Fibroblasts confirm the phenotype observed in HeLa

We then verified the effects we observed when we overexpressed the DNM2 CNM R465W mutation in mouse embryonic fibroblasts (MEF) from heterozygous mice and in fibroblasts from patients affected by CNM carrying the same mutation (Durieux et al., 2012; Durieux et al., 2010). As we observed in HeLa cells in overexpression studies above, mouse and human fibroblasts with endogenous heterozygous expression of this CNM mutation had increased LC3-II in basal but not under Bafilomycin A1 conditions (Fig. 7A and B), and increased of colocalisation of LC3 with RAB11A (Fig. S7A and B), suggesting defective release of LC3-positive structures from the RAB11A compartment. Depletion of ITSN1 in both human and mouse mutant fibroblasts restored normal autophagosome maturation in these mutant cells (increased LC3-II in absence/presence of Bafilomycin A (Fig. 7C and D)).

ITSN1 overexpression phenocopies DNM2 CNM mutation

If our hypothesis is correct, then overexpression of ITSN1 should negatively affect autophagy by sequestering DNM2 on the plasma membrane and phenocopy DNM2 loss of function as the CNM mutation. Consistent with this prediction, ITSN1 overexpression in normal cells blocked the release of LC3 from the recycling endosome compartment (increased colocalisation of LC3 on RAB11A (Fig. 7E-F and S7C), and increased recycling endosome tubulation/decreased fragmentation (increased numbers of cells with RAB11A tubules Fig. 7G). These phenotypes were associated with impaired autophagy, as measured by an increased percentage of cells with aggregates of mutant huntingtin exon 1 (Q74 aggregates (Fig. 7H)), an increase of LC3-II in basal conditions and not under Bafilomycin A1 (Fig. 7I) and a decrease of DNM2-LC3 binding (Fig. 7J).

DISCUSSION

Location, location, location

A major function of autophagy flux is to remove damaged mitochondria, altered proteins and unfolded proteins that are prone to aggregate. Indeed, muscles from

autophagy-defective mice (ATG7-/-, ATG5-/-) reveal degenerative changes, including vacuolated and centrally nucleated myofiber similar to that described for CNM (Masiero et al., 2009; Yoshii et al., 2016) . These studies reveal an unusual mechanism for the DNM2 R465W CNM mutation. This mutant protein is functionally normal in that it has the capacity to bind LC3 and can cause release of LC3/nascent autophagosomes from recycling endosomes. However, the mutation causes DNM2 sequestration to ITSN1 at the plasma membrane away from its LC3 binding sites at the recycling endosome - in this way it retains its functions in endocytosis but loses them in autophagy. This unusual mechanism for this mutation (which we have coined as the Location, location, location mechanism) may be more common, as many proteins have multiple potentially competing partners. Our data also suggest that the mutant protein acts as a dominant-negative for this autophagic process, as DNM2 oligomerises and we observed that overexpression phenocopied heterozygosity for the mutation and knockdown. This dominant-negative effect on autophagy is consistent with previous work showing that selective knockdown of the mutant allele in mice heterozygous for this mutation ameliorates their muscle phenotypes (Buono et al., 2018; Trochet et al., 2018).

This mutation also reveals a new step in autophagy – the release of LC3-positive nascent autophagosomes from RAB11A-positive recycling endosomes. DNM2 is normally recruited to this compartment via a LIR-dependent interaction with LC3 after LC3 is conjugated to these membranes. DNM2 regulates scission of the recycling endosomes and this appears to be specific to the membrane sites where LC3 is conjugated. This tubule scission thereby enables release of the LC3-positive autophagosomal structures. Previous literature has considered the key steps in autophagosome biogenesis to be induction, nucleation expansion and closure (Yin et al., 2016). We believe that “scission” from the core platform on which LC3 conjugation occurs, the RAB11A-positive recycling endosomes, should be added as a step, as this process is critical, it is defective in a human disease, and influences the way we consider how autophagosomes are formed. While we cannot exclude the possibility that this process may only have relevance to a subset of autophagosomes, we belive that it likely impacts most mammalian autophagosomes, since our previous data suggested that the RAB11A compartment and RAB11A-WIPI2 interactions are critical for autophagosome biogenesis (Puri et al., 2018a). Furthermore, our current

data suggest major disruptions to the autophagosome itinerary occur when DNM2-mediated RAB11A-compartment scission is perturbed, as assessed by autophagic substrate levels and quantitation the maturation of different autophagic structures by electron microscopy, LC3 blots, mRFP-GFP-LC3 and Halo-Tag assays.

ACKNOWLEDGMENTS

We thank Matthew Gratian, Mark Bowen for technical assistance, Antonina Andreeva (MRC Laboratory of Molecular Biology, Cambridge, UK) for useful discussions, Tamotsu Yoshimori (Osaka University, Japan), Mark McNiven (Mayo Clinic and Mayo Graduate School Rochester, Minnesota, USA), Anne Simonsen (Institute of Basic Medical Sciences-University of Oslo) for kindly providing reagents. Institute of Myology (Centre of Research in Myology, UMRS 974, F-75013, Paris, France) to provide the human fibroblasts from patients. We are grateful to the UK Dementia Research Institute (funded by the MRC, Alzheimer's Research UK and the Alzheimer's Society) (DCR) and The Roger de Spoelberch Foundation (DCR); Specialist Programme from Bloodwise (12048), the UK Medical Research Council (MC_U105161083, to AJW) (CH), Commonwealth Scholarships Commission UK (GMR).

AUTHOR CONTRIBUTIONS:

Conceptualization, DCR and CP; Methodology, CP; Investigation, CP; Writing – Original Draft, CP and DCR; Writing – Review & Editing, all authors; Funding Acquisition, DCR; Resources, YZ, MV, MM, GR, MB and KM; Supervision, DCR and CP.

Competing interests: FMM is employed by Eli Lilly and DCR is CSO of Aladdin Healthcare Technologies.

FIGURE LEGENDS

Figure 1: Recycling endosomes fragment to release autophagosomes

A) HeLa cells were fixed in basal conditions or after overnight treatment with HBSS (starved) and stained with RAB11A antibody. Histogram shows quantification of the percentage of cells showing RAB11A tubules in HeLa cells treated overnight with HBSS (starved), Rapamycin, or SMER28. Data are mean ± SD, (n=3; graphs represent means of the triplicates from three independent experiments); Two-tailed paired t test, **=p<0.01, ***=p<0.001.

B) HeLa cells were fixed in basal conditions or after 4 h of starvation in HBSS and labelled for RAB11A and LC3. In panel 1A left hand panel we have 3 cells which we scored as having tubules, while the cells in the right hand panel of Fig 1A were not considered to have this tubulation state.

C) HeLa cells were transfected for 24 h with pEGFP-RAB11A and mRFP-LC3 and processed for live imaging in HEPES-HBSS medium (See also Movie 1).

D) HeLa cells were transfected for 24 h with DNM2-pEGFP and mRFP-LC3, fixed in basal conditions and labelled for endogenous RAB11A. Histogram below shows quantification of the association of LC3 with DNM2 or DNM2 with RAB11A

E) HeLa cells were transfected for 24 h with DNM2-pEGFP were fixed in basal conditions and labelled for endogenous LC3 and RAB11A and processed for superresolution microscopy (SIM-Elyra). Left panel shows the structured illumination image, whilst right panel shows the isosurface rendering in which there is no transparency and colocalised pixels do not appear as yellow.

F) HeLa cells were transfected for 24 h with mCherry-RAB11A, DNM2-pEGFP and pECFP-LC3 and processed for live imaging in HEPES-HBSS medium.

The schematic diagram in the bottom shows outlines of the different channels in the different frames (See also Fig. S1B and Movie 2).

Figure 2: LC3 directly interacts with DNM2

A) HeLa cells transfected with control or DNM2 siRNA oligos (mix of oligos A and B) for 3 days, treated with DMSO (basal) or Bafilomycin A1 (Baf) for 4 h, processed for immunoblot and labeled for LC3, DNM2 and GAPDH as loading control. Histogram shows the relative amount of LC3-II in basal or under Baf treatment, normalized for GAPDH. Data are mean ± SD (n=3; graphs represent means of the

triplicates from three independent experiments) two-tailed paired *t*-test, ***=p<0.001, ns, not significant. The numbers indicate the LC3-II/GAPDH value of the shown experiment.

B-D) HeLa cells transfected with control or DNM2 siRNA oligos (mix of oligos A and B) for 3 days, fixed and labelled for endogenous LC3 and RAB11A. The histogram in **B** shows the percentage of cells with RAB11A tubules; the histogram **C** shows the quantification of the association of LC3 with RAB11A (Manders' Coefficient). Data are mean ± SD (n=3; graphs represent means of the triplicates from three independent experiments). Two-tailed paired t test, **=p<0.01.

E-F) HeLa cells were transfected with GFP-LC3 for 20h and treated for 1 h with Bafilomycin A1 followed by 4h in HBSS (starvation), Rapamycin (RAP) (1 μM), or SMER28 (20 μM). Immunoprecipitates obtained by GFP-TRAP were processed for immunoblot for DNM2. The amount of DNM2 co-immunoprecipitated with EGFP-LC3 was quantified and normalized for the amount of LC3 immunoprecipitated. Data are mean ± SD (n=4; graphs represent means of four independent experiments). Two-tailed paired t test, **=p<0.01.

G) Recombinant DNM2 and LC3 proteins were incubated for 1 h at 25°C with gentle shaking. The mixture of the two proteins was immunoprecipitated using anti-DNM2 antibody and blotted for LC3 and DNM2. As control we immunoprecipitated DNM2 alone or LC3 alone. Note that recombinant LC3 levels in the input were below detection levels by western blotting.

H) Representation of the different domains of DNM2. The LIR, identified using ILIR software (Jacomin et al., 2016), is shown.

I) HeLa cells were transfected with DNM2 siRNA (oligo A and oligo B (see material and methods)) for 3 days. DNM2-silenced HeLa cells were transfected in the last 20 h with pEGFP-empty vector or with pEGFP-LC3 and HA-DNM2-WT or W525L. Immunoprecipitates obtained by GFP-TRAP were processed for immunoblot for DNM2. The histogram shows the amount of DNM2 co-immunoprecipitated with EGFP-LC3 normalized for the amount of LC3 immunoprecipitated. Data are mean ± SD (n=4; graphs represent means of the triplicates from three independent experiments). Two-tailed paired t test, ****=p<0.0001.

J) HeLa cells were silenced with siRNAs to DNM2 for 3 days and transfected for the last 20 h with NM2-pEGFP-WT or W525L.The cells were fixed and labelled for endogenous LC3 and RAB11A. The histogram on the left shows the percentage of

cells with RAB11A tubules. The histogram on the right shows the quantification of the association of LC3 with RAB11A or DNM2 with RAB11A (Manders' Coefficient). Data are mean ± SD (n=3 graphs represent means of the triplicates from three independent experiments). Two-tailed paired t test, *=p<0.05, **=p<0.01.

K) HeLa cells transfected with DNM2 siRNA oligos (mix of oligos A and B) for 3 days, transfected for the last 20 h with HA-DNM2-WT or W525L, treated with DMSO (basal) or Bafilomycin A1 (Baf) for 4 h, processed for immunoblot and labeled LC3, DNM2 and GAPDH as loading control. Histogram shows the relative amount of LC3-II in basal or under Baf treatment normalized for GAPDH. Data are mean ± SD (n=3; graphs represent means of the triplicates from three independent experiments) two-tailed paired *t*-test, **=p<0.01, ns, not significant. The numbers indicate the LC3-II/GAPDH value of the shown experiment.

L) Ribbon representation of LC3B (PDB code: 5w9a) docked onto the PH domain of dynamin (PDB code: 5a3f). LC3B is coloured green and PH domain of dynamin is coloured cyan. Conserved LC3 residue R70 is coloured in magenta and K51 is coloured in orange. DNM2 W525 residue is coloured in yellow. The figure was prepared using the program PyMOL (http://www.pymol.org).

M) HeLa cells were transfected for 20 h with pEGFP-LC3-WT, or K51A, or R70A. Immunoprecipitates obtained by GFP-TRAP were processed for immunoblot for DNM2. P62 was used as control. The histograms show the amount of DNM2 or P62 co-immunoprecipitated with EGFP-LC3, normalized for the amount of LC3 immunoprecipitated. Data are mean ± SD (n=3 graphs represent means of the triplicates from three independent experiments). Two-tailed paired t test, ****=p<0.0001, **=p<0.01, ns, not significant.

Figure 3: Cells expressing DNM2 R465W accumulate immature autophagosomes

A-B) WT or Fibroblast from patients carrying DNM2 R465W mutation and HeLa stable cell lines expressing DNM2 WT or DNM2 R465W mutation were starved 1 h and fixed for electron microscopy. The number of phagophore/autophagosomes (Ph/Au) or autolysosomes (AL) on 10 cells profiles were quantified. The histogram shows the number of structures/cell. Data are mean ± SD (n=10 cells each condition) two-tailed paired *t*-test, ***=p<0.001, ****=p<0.0001.

Bottom panels of A show the EM images of the mutant (middle panels) outlining the autophagosomes (green) and the nearby tubules, which may be recycling endosomes.

Figure 4: Cells expressing DNM2 R465W accumulate autophagosomes on recycling endosomes

A) HeLa cells were transfected with pEGFP-empty or pEGFP-DNM2 -WT or R465W in combination with HA-tagged Htt-Q74 (mutant form of huntingtin associated with Huntington's disease) for 24 h and processed for immunofluorescence. Numbers of cells with Htt-Q74 aggregates are shown. Data are mean ± SD (n=3, graphs represent means of the triplicates from three independent experiments). Two-tailed paired t test, ***=p<0.001.

B) HeLa cells were transfected for 20 h with pEGFP-empty vector, or with pEGFP-LC3 and HA-DNM2-WT or HA-DNM2-R465W. Immunoprecipitates obtained by GFP-TRAP were processed for immunoblot for anti-HA. Note input is on right hand side of the gel. The histogram shows the amount of HA-DNM2 co-immunoprecipitated with pEGFP-LC3, normalized for the amount of LC3 immunoprecipitated. Data are mean ± SD (n=3; graphs represent means of the triplicates from three independent experiments). Two-tailed paired t test, **=p<0.01.

C) HeLa cells were transfected for 20 h with HA-DNM2-WT or R465W. The cells were fixed and labelled for anti-HA and endogenous LC3 and RAB11A. The histogram below on the right shows the quantification of the association of LC3 with DNM2 or LC3 with RAB11A (Manders' Coefficient). The histogram on the left shows the percentage of cells with RAB11A tubules; Data are mean ± SD (n=3; graphs represent means of the triplicates from three independent experiments). Two-tailed paired t test, **=p<0.01, ***=p<0.001.

D) HeLa cells were transfected for 20 h with pEGFP-DNM2 -WT or R465W. The cells were fixed and labelled for endogenous RAB11A. The histogram on the left shows the quantification of the association of DNM2 with RAB11A (Manders' Coefficient). Data are mean ± SD (n=3; graphs represent means of the triplicates from three independent experiments). Two-tailed paired t test, ***=p<0.001.

E) HeLa cells transfected for 20 h with pEGFP-DNM2-WT or R465W were treated with DMSO (basal) or Bafilomycin A1 (Baf) for 4 h, processed for immunoblot and labeled LC3, DNM2 and GAPDH as loading control. The histogram shows the relative amount of LC3-II in basal or under Baf treatment normalized for GAPDH. Data are mean ± SD (n=3; graphs represent means of the triplicates from three independent experiments) two-tailed paired *t*-test, **=p<0.01, ns, not significant. The

numbers indicate the LC3-II/GAPDH value of the shown experiment.

Figure 5: Cells expressing DNM2 mutants accumulate immature autophagosomes

A) HeLa cells were transfected for 20 h with HA-DNM2-WT or HA-DNM2-R465W or HA-DNM2-W525L and pEGFP-RAB11A and labelled for anti-HA and anti-ATG9A or anti-ATG16L1. The colocalization between ATG9A or ATG16L1 with RAB11A were quantified and shown in Fig. S7A.

B) HeLa cells stably expressing DNM2 -pEGFP WT, DNM2 -pEGFP R465W or DNM2 -pEGFP W525L were starved for 1 h in HBSS, loaded with Ferrofluid-anti-ATG9A antibody for 1 h in HBSS and chased for 15 min in HBSS. The cells were then fragmented and the membranes containing Ferrofluid-anti-ATG9A (Bound) or not containing Ferrofluid-anti-ATG9A (Unbound) were separated, lysed and processed for immunoblotting as indicated (see technical details in Material and Methods).

C) HeLa stable cell line expressing the tandem tagged mRFP-GFP-LC3 were transfected for 20 h with HA-DNM2 WT or HA-DNM2 R465W or HA-DNM2-W525L and labelled with anti-HA to visualize the transfected cells. The number of total vesicles or red-only vesicles were quantified and shown in Fig. S5G.

D-E) U-2 OS cells stably expressing HaloTag-LC3 (HT-LC3) were transfected for 20 h with HA-DNM2 WT or HA-DNM2 R465W or HA-DNM2-W525L and loaded with a combination of membrane-impermeable Alexa Fluor (AF) 488 HaloTag ligand (MIL) and membrane-permeable tetramethylrhodamine HaloTag ligand (MPL) and labelled for anti-HA. MIL+MPL (phagophores), MIL+MPL+ (nascent autophagosomes), MIL−MPL+ (mature autophagosomes, and autolysosomes) were quantified in HA-positive cells. The histogram in E shows the number of structures/cell. Data are mean ± SD (n=10 cells each condition) One-way ANOVA with post hoc Tukey's test, **=$p<0.01$, ****=$p<0.0001$, ns= not significant.

F) HeLa cells stably expressing DNM2-pEGFP-WT (wild-type), -R465W or -W525L were processed for western blot to analyze the amount of pro- or mature Cathepsin D. The ratio of mature vs total Cathepsin D were analyzed and the results are shown in Fig. S5H.

Figure 6: ITSN1 sequesters DNM2 R465W on plasma membrane

A) HeLa cells transfected with pEGFP-DNM2-WT or R465W for 24 h were fixed and treated for immunogold labelling on cryosections. EGFP-DNM2 was detected with anti-GFP antibody (15 nm gold). The number of DNM2 "plaques" on the plasma membrane present on 10 cells profiles were quantified. The histogram shows the number of DNM2 "plaques" on plasma membrane/cell. Data are mean ± SD (n=10 cells each condition) two-tailed paired *t*-test, ***=p<0.001.

B) HeLa cells were transfected with pEGFP-empty or pEGFP-DNM2-WT or -R465W for 24 h, fixed and labelled for endogenous AP2 and processed for Total Internal Reflection Fluorescence (TIRF). The histogram on the right shows the quantification of the association of DNM2 with AP2 (Pearson's Correlation). Data are mean ± SD (n=7 cells each condition). Two-tailed paired *t*-test, **=p<0.01.

C-D) HeLa cells were transfected for 20 h with empty vector or with HA-DNM2-WT or R465W. The lysates were immunoprecipitated with anti-HA-conjugated magnetic beads and processed for immunoblot for anti-ITSN1. The histogram shows the amount of ITSN1 co-immunoprecipitated with HA-DNM2-, normalized for the amount of HA-DNM2 immunoprecipitated. Data are mean ± SD (n=3 graphs represent means of the triplicates from three independent experiments). Two-tailed paired t test, **=p<0.01.

E) HeLa cells transfected with control or ITSN1 siRNA oligos for 3 days were transfected for 20 h with HA-DNM2 R465W. The cells were fixed and labelled for anti-HA and endogenous LC3 and RAB11A. The histogram shows the percentage of cells with RAB11A tubules. Data are mean ± SD (n=3, graphs represent means of the triplicates from three independent experiments). Two-tailed paired t test, **=p<0.01. See also Fig. S4A.

F) HeLa cells transfected with control or ITSN1 siRNA oligos for 3 days were transfected in the last 20 h with HA-DNM2 WT or R465W. The cells were fixed and labelled for endogenous AP2 and processed for Total Internal Reflection Fluorescence (TIRF). The histogram in Fig. S6C shows the quantification of the association of DNM2 with AP2 (Pearson's Correlation).

G) HeLa cells transfected with control or ITSN1 siRNA oligos for 3 days were transfected in the last 20 h with HA-DNM2 WT or R465W. The cells were labelled for endogenous RAB11A and LC3 and visualised on Elyra (Zeiss) superresolution

microscope. Top panels show the structured illumination image, whilst bottom panels show the isosurface rendering.

H) HeLa cells transfected with control or ITSN1 siRNA oligos for 3 days, then transfected in the last 20 h with HA-DNM2 R465W and pEGFP-LC3 or empty pEGFP vector. Immunoprecipitates obtained by GFP-TRAP were processed for immunoblot for anti-HA. The histogram below shows the amount of HA-DNM2 co-immunoprecipitated with EGFP-LC3, normalized for the amount of EGFP-LC3 immunoprecipitated. Data are mean ± SD (n=3 graphs represent means of the triplicates from three independent experiments). Two-tailed paired t test, ****=p<0.0001.

I) HeLa cells transfected with DNM2 and control or ITSN1 siRNA oligos for 3 days, were then transfected in the last 20 h with HA-DNM2 R465W. The cells were treated with DMSO (basal) or Bafilomycin A1 (Baf) for 4 h, processed for immunoblot and labeled LC3, HA-DNM2 and GAPDH as loading control. The histogram shows the relative amount of LC3-II in basal or under Bafilomicyn A1 (Baf) treatment, normalized for GAPDH. Data are mean ± SD (n=3, graphs represent means of the triplicates from three independent experiments) two-tailed paired *t*-test, **=p<0.01, ***=p<0.001. The numbers indicate the LC3-II/GAPDH value of the shown experiment.

J) HeLa cells transfected with DNM2 and control or ITSN1 siRNA oligos for 3 days, were then transfected in the last 20 h with HA-DNM2 W525L. The cells were treated with DMSO (basal) or Bafilomycin A1 (Baf) for 4 h, processed for immunoblot and labeled for LC3, HA-DNM2, and GAPDH as loading control. The histogram shows the relative amount of LC3-II in basal or under Baf treatment normalized for GAPDH. Data are mean ± SD (n=3, graphs represent means of the triplicates from three independent experiments) two-tailed paired *t*-test, ns, not significant. The numbers indicate the LC3-II/GAPDH value of the shown experiment.

Figure 7: R465W Fibroblasts confirm the phenotype observed in HeLa and overexpression of ITSN1 mimics the phenotype of DNM2 R465W mutant

A-B) WT human fibroblasts and R465W mutant (from CNM patient) or WT or R465W heterozygous (HET) mouse embryonic fibroblasts (MEFs) were treated with DMSO (basal) or Bafilomycin A1 (Baf) for 4 h, processed for immunoblot and labeled LC3 and GAPDH as loading control. Histograms shows the relative amount

of LC3-II in basal or Baf treatment normalized for GAPDH. Data are mean ± SD (n=3; graphs represent means of the triplicates from three independent experiments). Two-tailed paired *t*-test, **=p<0.01, ns, not significant. The numbers indicate the LC3-II/GAPDH ratios of the representative blots.

C-D) WT human fibroblasts and R465W mutant (from CNM patient) or WT or R465W HET MEF transfected with control or ITSN1 siRNA oligos for 3 days. The fibroblasts were then treated with DMSO (basal) or Bafilomycin A1 (Baf) for 4 h, processed for immunoblot and labeled LC3 and GAPDH as loading control. The histogram shows the relative amount of LC3-II in basal or under Baf treatment normalized for GAPDH. Data are mean ± SD (n=3, graphs represent means of the triplicates from three independent experiments) two-tailed paired *t*-test, *=p<0.05, **=p<0.01, ****=p<0.0001. The numbers indicate the LC3-II/GAPDH values of the representative blots.

E-G) HeLa cells were transfected for 20 h with pEGFP-ITSN1 or pEGFP empty vector. The cells were fixed for endogenous LC3 and RAB11A. The histogram in **F** shows the quantification of the association of LC3 with RAB11A (Manders' Coefficient). The histogram in **G** shows the percentage of cells with RAB11A tubules; Data are mean ± SD (n=3, graphs represent means of the triplicates from three independent experiments). Two-tailed paired *t* test, *=p<0.05, **=p<0.01.

H) HeLa cells were transfected with pEGFP-ITSN1 or pEGFP empty vector in combination with HA-tagged Htt-Q74 (mutant form of huntingtin associated with Huntington's disease) for 24 h and processed for immunofluorescence. The percentages of cells with Htt-Q74 aggregates is shown. Data are mean ± SD (n=3; graphs represent means of the triplicates from three independent experiments). Two-tailed paired t test, *=p<0.05.

I) HeLa cells transfected for 20 h with flag-ITSN1 or flag-empty vector were treated with DMSO (basal) or Bafilomycin A1 (Baf) for 4 h, processed for immunoblot and labeled anti-Flag, LC3 and GAPDH as loading control. The histogram shows the relative amount of LC3-II in basal or under Baf treatment normalized for GAPDH. Data are mean ± SD (n=3; graphs represent means of the triplicates from three independent experiments). Two-tailed paired *t*-test, ****=p<0.0001, ns, not significant. The numbers indicate the LC3-II/GAPDH values of the representative blot.

J) HeLa cells transfected for 20 h with flag-ITSN1 or empty-flag vector and pEGFP-

LC3 or pEGFP empty vector. Immunoprecipitates obtained by GFP-TRAP were processed for immunoblot for DNM2. The histogram shows the amount of DNM2 co-immunoprecipitated with pEGFP-LC3 normalized for the amount of EGFP-LC3 immunoprecipitated. Data are mean ± SD (n=3 graphs represent means of the triplicates from three independent experiments). Two-tailed paired t test, ***=p<0.001.

STAR Methods text

RESOURCE AVAILABILITY

Lead Contact

Further information and requests for resources and reagents should be directed to and will be fulfilled by the Lead Contact, David C Rubinsztein (dcr1000@cam.ac.uk).

Materials Availability Statement

Plasmids generated in this study will be deposited to Addgene. In the meanwhile, we will make plasmids and cell lines that we have generated available through requests to the lead contact/corresponding author.

Data and Code Availability Statement

This study did not generate datasets or code.

EXPERIMENTAL MODEL AND SUBJECT DETAILS

Cell Culture

HeLa cells were cultured in Dulbecco's modified Eagle's medium (DMEM) (SIGMA D6548) supplemented with 2 mM L-glutamine, 100 U/ml Penicillin/Streptomycin and 10% Fetal Bovine Serum in 5% CO_2 at 37°C. Human fibroblasts and Mouse Embryonic Fibroblasts (MEF) were cultured in Dulbecco's modified Eagle's medium-GlutMAX (Gibco 31966) supplemented with 2 mM L-glutamine, 100 U/ml Penicillin/Streptomycin and 20% Fetal Bovine Serum, Sodium Pyruvate (SIGMAS8636) and Non-essential amino acids (SIGMA M7145).

Stable cell line

U2OS Halotag-LC3

Halotag-LC3 (MAP1LC3B) constructs were purchased from the Kazusa collection (Promega). Plasmid DNA was digested with Sco1 and the linear DNA fragment encoding the tagged LC3 along with the CMV promoter was gel-extracted. U2OS cells were grown in a 6 well plate until 80% confluent and cells were transfected with 1ug linear plasmid DNA, 100 ng linear hygromycin marker (Clontech) 10 ug Nupherin and 4 ul Mirus transfection reagent per well, and in control wells no DNA was added. When confluent, each well was split into a 10 cm culture dish and media was supplemented with 100 ug/ml hygromycin. Cells were maintained until all cells in control dishes were dead. In order to generate single cell clones, cells in culture were labelled with diAcFam Halotag ligand (Promega) following manufacturer's instructions. Halotag expressing (labelled) cells were selected by FACS and sorted into 96 well plates with one cell per well. Single cells were then expanded to generate clonal cell lines. Expression of Halotag-LC3 was confirmed by two methods; cells were lysed and assessed by western blotting using LC3 antibody to confirm the presence of a band at the expect molecular weight, and cells were labelled with TMR Halotag ligand (Promega), lysed and run on an agarose gel. The gel was then scanned on a Typhoon Trio Imager Scanner to detect the fluorescently labelled Halotag protein and confirm the molecular weight.

HeLa DNM2-PEGFP WT and mutants

HeLa cells were transfected with GFP- DNM2-PEGFP WT and mutant constructs (Puri et al., 2013). After 24 h, the cells were placed in selection medium (DMEM supplemented with 0.5 μg/ml G418) for 10 days. The antibiotic-resistant cells were then FACS sorted to isolate the GFP-expressing population. The cells were maintained in culture with DMEM supplemented with 0.5 μg/ml G418. HeLa cells stably expressing GFP- DNM2-PEGFP WT and mutants were maintained in culture with DMEM supplemented with 0.6 μg/ml G418, as previously described (Ravikumar et al., 2010).

METHOD DETAILS

Antibodies and reagents

The antibodies used were: mouse anti AP2 (AP6 clone MA1-064 Thermofisher 1: 200 for IF), rabbit anti-ATG3 (ab108251-ABCAM; 1:200 for IF), rabbit anti-ATG9A (ab108338-ABCAM 1:200 for IF), rabbit anti-ATG16L1 (D6D5-Cell Signaling f; 1:200 for immunofluorescence), mouse anti-Cathepsin D (ab6313- ABCAM for WB 1:100), rabbit anti DNM2 (ab65556 ABCAM 1:1000 immunoblot), mouse anti-Flag (clone M2 SIGMA F1804 1:100 for immunoblot), rabbit anti-GABARAP (AP1821A-GENERON; for IP 1:140 and WB1:1000), rabbit anti-GABARAP-L1 (110101-Proteintech; for IP 1:140 and WB1:1000), rabbit anti-GABARAP-L2 (PM038-MBL; for IP 1:140 and WB1:1000), mouse anti-GAPDH (ab8245-ABCAM; 1:5000 for immunoblot), rabbit anti-GFP (A6455-Invitrogen; 1:100 for EM), mouse anti-HA (16B12- Biolegend; 1:400 for IF and immunoblot), rabbit anti-ITSN1 (ABN1378 Millipore 1:100 immunoblot), mouse anti-LC3B (0231-100/LC3-5F10-Nanotools; 1:200 for IF), rabbit anti-LC3B (ab192890-ABCAM; 1:200 for IF and immunoblot), rabbit anti-P62 (MBL PM045; 1:1000 for immunoblot), mouse anti-Myc tag(ab18185-ABCAM), rabbit anti-RAB11A (ab128913-ABCAM; 1:1000 for immunoblot and 1:200 for IF), Ferrofluid EMG508 is from Megatech ltd. (TSD-06-24-11-1). GFP-TRAP and Myc-TRAP are from Chromotek, Anti-HA Magnetic Beads (Pierce 88836). Protein-A gold is from CMC (Utrecht- NL), human transferrin Alexa-647 (T23366) and Alexa-488 (T13342) (Thermofisher), HaloTag TMR ligand (Promega G825A), HaloTag Alexa 488 ligand (Promega G100A) and Seahorse XF Plasma membrane permeabilizer (Agilent Technologies 102504-100).

All the secondary antibodies for immunofluorescence and LICOR are from Thermofisher.

Drug treatments used include: 400 nM Bafilomycin-A1 (Enzo, BML-CM110).

The rabbit antibody anti-ATG9A (1963) (aa 42-57 in the loop 2: Ac-SRLNRGYKPASKYMNC -NH2) was made by Eurogentec (for FerroFluid 1:20 (100 ul in 2 ml Serum free medium with 5 ul FerroFluid) and WB 1:1000).

Plasmids

pEGFP-RAB11A, mCherry-RAB11A, have been described elsewhere (Puri et al., 2013); pEGFP-LC3, pECFP-LC3, mRFP-LC3 were a kind gift from Tamotsu Yoshimori (Osaka University, Japan), LC3-PGEX-6P-1 was a gift from Mineyuki Mizuguchi (Faculty of Pharmaceutical Sciences, Toyama Medical and Pharmaceutical

University, Laboratory of Structual Biology), DNM2-WT-PEGFP- was a gift from Mark McNiven (Mayo Clinic and Mayo Graduate School Rochester, Minnesota, USA), HA -DNM2-WT (Addgene-34684), Flag-ITSN1-short (Addgene 47392), pEGFP-ITSN1 short (Addgene 47394), Flag-empty vector (SIGMA-E4901), Myc-SNX18-WT and W38F was a kind gift from Anne Simonsen (Institute of Basic Medical Sciences- University of Oslo).

Mutagenesis

All LC3 and DNM2 mutant were generated by using a QuikChange Lightning Multisite-Directed Mutagenesis kit (Agilent Technologies 210515-5) according to the manufacturer's instructions.

Cell transfection

The cells were seeded at 1-2 x105 per 6-well and transfections were performed using LipofectAMINE 2000 for siRNA, according to the manufacturer's instructions, using 100 nM siRNA. All the DNA constructs were transfected using Mirus Bio TransIT ®-2020, at 1 μg per well of a 6-well plate.

Western blot analysis

HeLa cells were lysed in Laemmli buffer. Protein samples were boiled for 5–7 minutes at 100°C, separated by SDS-PAGE, transferred onto PVDF membranes, then subjected to western blot analysis. The membrane were labelled with fluorescent secondary antibody and analysed with a LICOR-Odyssey apparatus using IMAGE STUDIO Lite software, which enables quantitative analysis of blotting signals.

Immunoprecipitation

HeLa cells were treated as described in Figure legends and lysed in lysis buffer (50 mM Hepes, 50 mM NaCl, 10% glycerol, 1% Triton X-100, 1.5 mM MgCl, 5 mM EGTA)) for 15 min on ice and pelleted for 10 min at 13.000 rpm. The supernatant was incubated with the LC3 antibody (ab192890-ABCAM) or control IgG antibodies (2729S Cell Signaling) (1:100) for 3 h and 2 h with Dynabeads Protein A (Novex-Lifechnologies). The immunoprecipitate was eluted by boiling the samples in Laemmli buffer for 5 min. EGFP-tagged proteins (DNM2-pEGFP and pEGFP-LC3) were pulled down using GFP-TRAP beads (ChromoTek) according to the

manufacturer's protocol. Proteins were resolved by SDS-PAGE. Similarly was done for Myc-TRAP.

Immunofluorescence Microscopy

Cells grown on coverslips at 25% confluency were fixed in 4% paraformaldehyde for 5 minutes, then permeabilised with 0.1% Triton or methanol. 1% BSA in PBS was used for blocking and for primary and secondary antibody incubations. The experiments visualizing endogenous LC3 were fixed with methanol for 5 minutes at -20°C. A Zeiss LSM710 confocal microscope was used for fluorescent confocal analysis. All confocal images were taken with a 63× oil-immersion lens.

HaloTag-LC3

The HaloTag-LC3 autophagosome completion assay was performed as previously described by Takahashi et al (Takahashi et al., 2018). Briefly, HaloTag-LC3 expressing cells were transfected with HA-DNM2-WT or mutants for 20 h on Matek 35 mm dishes (MatTek, Ashland MA USA ; P35G-1.0-14-C) and incubated in MAS buffer (220 mM mannitol, 70 mM sucrose, 10 mM KH2PO4, 5 mM MgCl2, 2 mM HEPES, 1 mM EGTA) containing Seahorse XF-PMP (Agilent-1025 04 100) (2–3 nM) and MIL (Promega-G100A) at 37 °C for 15 min. Cells were then fixed in 4% PFA for 5 min, washed three times in PBS, and incubated with mouse anti-HA antibody (Biolegend- 901501) for 1 h at room temperature. The cells were then incubated by goat anti-mouse Alexa 647 antibody and MPL (Promega- G825A) for 30 min. Imaging was performed on an incubated Zeiss AxioObserver Z1 microscope with a LSM780 confocal attachment using a 63× 1.4 NA Plan Apochromat oil-immersion lens.

Aggregate quantification

The httQ74-HA aggregation was detected by immunofluorescence (primary HA antibody). The proportion of transfected cells with aggregates was scored (approx. 500 cells per coverslip). Experiments were performed blinded and in triplicate in at least three independent experiments. Statistics for aggregation assays were calculated as odds ratios.

Live Cell Imaging

HeLa cells were seeded on MatTek Petri dishes (MatTek, Ashland MA USA) at a density of approximately 1.5×10^5 cells per dish. Cells were placed in HBSS with HEPES, after which they were imaged immediately at 37°C. Each frame was 4.2 seconds. Imaging was performed on an incubated Zeiss AxioObserver Z1 microscope with a LSM780 confocal attachment using a 63× 1.4 NA Plan Apochromat oil-immersion lens.

Superresolution microscopy

Samples were stained for conventional fluorescence microscopy and mounted on high-precision size 1.5 coverslips (Carl Zeiss Ltd, Cambridge). Coverslips were mounted with ProLong Gold anti-fade medium (Life Technologies, P36934), which was left to cure for 3 days at room temperature in order to produce samples with a consistent refractive index. Super-Resolution Structured Illumination Microscopy (SR-SIM) was performed using an Elyra PS1 instrument (Carl Zeiss Ltd). Samples were examined on the microscope using a 63x 1.4NA plan-apo Carl Zeiss objective lens and Immersol 518F (23ºC) immersion oil. Image acquisition was carried out using ZEN 2012 Elyra edition software in which data sets were collected with 5 grating phases, 5 rotations and sufficient z positions spaced 110 nm apart to form an approximately 2 μm deep volume of raw SR-SIM data. Optimal grating frequencies were selected for each wavelength used. Structured Illumination post-processing was performed in ZEN using parameters determined by automated analysis of the datasets. Reconstructed images were then corrected for spherical and chromatic aberrations using channel alignment information, which was created using a 3D array of multi-spectral beads previously imaged with the same instrument settings. The average final image resolution was calculated to be 110 nm in x and y dimensions and 240 nm in the z dimension which represents a two-fold lateral and axial improvement in resolution compared to conventional microscopy.

Electron Microscopy

HeLa cells stably expressing DNM2-EGFP WT or R465W and Fibroblasts from a patient carrying the DNM2 R465W mutation (Buono et al., 2018; Trochet et al., 2018) or a unaffected control were then placed at 37°C in HBSS for 1 h and fixed in a

mixture 2% Paraformaldehyde and 2% Glutaraldehyde in 0.1 M cacodylate buffer (pH 7.4) for 1 h at room temperature. The cells were then post-fixed in 1% Osmium Tetroxide in 0.1 M cacodylate buffer (pH 7.4) for 20 min and processed for standard Epon embedding. The sections were observed using a Philips CM100 or FEI Tecnai Spirit electron microscopes.

Immunogold Electron Microscopy

Immunogold on cryosections. HeLa cells were transfected with pEGFP-DNM2-WT or R465W for 24 h and fixed with a mixture of 2% paraformaldehyde and 0.2% glutaraldehyde in phosphate buffer (pH 7.4) for 2 h, at room temperature. Cells were then prepared for ultrathin cryosectioning and immunogold-labelled, as previously described (Puri et al., 2013). Briefly, fixed cells were washed once in PBS/0.02 M glycine, after which cells were scraped in 12% gelatin in PBS and embedded in the same solution. The cell-gelatin was cut into 1 mm blocks, infiltrated with 2.3 M sucrose at 4°C overnight, mounted on aluminium pins and frozen in liquid nitrogen. Ultrathin cryosections were picked up in a mixture of 50% sucrose and 50% methylcellulose and incubated with primary antibodies (rabbit anti-GFP) followed by protein A gold (Utrecht)(Puri et al., 2013).

FerroFluid

Tf-enriched membrane isolation using Magnetic Microbeads (Ferrofluid) was performed as previously described (Puri et al., 2018a). Similar approach was used with anti ATG9A antibody (1963-Eurogentech).

FACS-based endocytosis assays

Transferrin-endocytosis assay was performed as previously described (Peden et al., 2004). Briefly, the cells were incubated for different time points (5 min, 10 min, 15 min and 20 min) in presence of Tf–Alexa-Fluor-647. Cells were then washed for various times before fixation in 4% paraformaldehyde in PBS. Cell-associated Tf–Alexa-Fluor-647 was determined by FACS analysis using BD FACSCalibur flow cytometer (BD Biosciences) and FlowJo software (Tree Star Inc.).

Purification of recombinant LC3

LC3 was purified as described (Yin et al., 2016) with some modifications. Briefly, LC3B was expressed using a pGEX-6p1 plasmid in E coli for 3 h at 37°C after induction with 1 mM IPTG. Cells were lysed in 50 mM Tris pH 7.4, 150 mM NaCl using a sonicator in the presence of proteases inhibitors and centrifugated at 40,000 rpm for 30 min at 4°C. The supernatant was incubated with glutathione-Sepharose 4B beads followed by extensive washes in lysis buffer. PreScission Protease (GE Healthcare, 27-0843-01) was added at 100 units/ml in a 2-bed volume of PreScission Buffer (50 mM Tris-HCl pH 7.5, 150 mM NaCl, 1 mM EDTA) freshly prepared with 1 mM DTT and cleavage was performed overnight at 4°C. Cleaved protein was eluted and stored at -80°C.

Protein binding assay.

Binding of LC3B (purified from E.Coli) to DNM2 (Origene, TP323585) was performed by incubation of recombinant proteins at 25^0C for 1 h, followed by immunoprecipitation with rabbit anti-DNM2 antibody (ABCAM, ab65556-1:700) and processed for western blot analysis.

QUANTIFICATION AND STATISTICAL ANALYSIS

Image analysis

Volocity software (PerkinElmer) was used for analysis and processing of confocal images. For co-localization analysis of confocal images, we used Manders' Coefficient. All experiments were repeated at least three times. The background was fixed for all within-experiment analyses. Volocity software was also used for the Z stack reconstruction; the images presented also include the isosurface rendering in which there is no transparency and colocalised pixels do not appear as yellow.

For analysis of SIM images, final visualisation and video production was performed in Volocity 6.3 Software using isosurface rendering of selected cropped regions of the datasets. Isosurface rendering was used to more clearly visualise the shapes of fluorescent structures within the complex fluorescence volume datasets. This rendering type produces a three-dimensional surface contour connecting points in space which have the same fluorescence intensity value (a threshold value), this value defines what is inside or outside of an object and allows us to visualise the point where the signal rises above background values. Structures rendered in this way

appear solid and therefore what is inside or behind them is hidden from the viewer's perspective. It is not possible to directly observe colocalisation of signals in such images, instead we simply visualise the contact and overlap of the object's shapes.

In all the experiments in which we quantified the percentage of cells with RAB11A tubules we analysed how many cells had RAB11A in tubulation states compared with the total. In panel 1A left hand panel we have 3 cells which we scored as having tubules, while the cells in the right hand panel of Fig 1A were not considered to have this tubulation state. We always analysed at least 250 cells in duplicate per experiment, in each condition, in three independent experiments. The quantification was done directly on the microscope with the identity of the slides blinded to the person doing the analysis.

Statistics

Significance levels for comparisons between two groups were determined with t test (2-tailed). *= $p \leq 0.05$; **= $p \leq 0.01$; ***= $p \leq 0.001$. A P value of 0.05 was considered as the borderline for statistical significance.

For experiments where we have considered data from multiple independent experiments, we have normalised control data and used 1-sample t tests. For LC3-II blots, we have normalised both basal and bafilomycin A1 data.

For some experiments where we have assessed colocalisations in different conditions or western blot analysis, we have reported data from representative single experiments and noted cell numbers in the legends. This approach was used to minimise effects of heterogeneity between experiments.

Excel and Prism 7 software were used for statistical analysis and generation of graphs. See details in the figure legends.

SUPPLEMENTAL ITEMS

Supplementary Tables

Table S1 (related to Key Resources table): siRNA sequences

Supplementary video legends

Movie 1 (Related to Figure 1C): LC3 emerges from RAB11A-positive tubule and is released upon RAB11A tubules fragmentation. Confocal live imaging of HeLa expressing the recycling endosome marker pEGFP-RAB11A and the autophagosome marker pECFP-LC3. Cells were moved to HBSS-HEPES media and imaged for 15 min.

Movie 2 (Related to Figure 1F): DNM2 localises between LC3 and the RAB11A-positive tubule before the autophagosomes releases. Confocal live imaging of HeLa expressing the recycling endosome marker mCherry-RAB11A, the autophagosome marker pECFP-LC3 and DNM2-pEGFP-WT. Cells were switched to HBSS-HEPES media and imaged for 15 min.

Movie 3 (Related to Figure S3C and 5E): In absence of DNM2 on recycling endosomes, the LC3 structures unable to detach from the RAB11A-positive tubule moving along the tubule. Confocal live imaging of HeLa expressing the recycling endosome marker mCherry-RAB11A, the autophagosome marker pECFP-LC3 and DNM2-pEGFP-R465W. Cells were switched to HBSS-HEPES media and imaged for 15 min.

REFERENCES

Ali, T., Bednarska, J., Vassilopoulos, S., Tran, M., Diakonov, I.A., Ziyadeh-Isleem, A., Guicheney, P., Gorelik, J., Korchev, Y.E., Reilly, M.M., *et al*. (2019). Correlative SICM-FCM reveals changes in morphology and kinetics of endocytic pits induced by disease-associated mutations in dynamin. FASEB J, fj201802635R.

Antonny, B., Burd, C., De Camilli, P., Chen, E., Daumke, O., Faelber, K., Ford, M., Frolov, V.A., Frost, A., Hinshaw, J.E., *et al*. (2016). Membrane fission by dynamin: what we know and what we need to know. EMBO J *35*, 2270-2284.

Axe, E.L., Walker, S.A., Manifava, M., Chandra, P., Roderick, H.L., Habermann, A., Griffiths, G., and Ktistakis, N.T. (2008). Autophagosome formation from membrane compartments enriched in phosphatidylinositol 3-phosphate and dynamically connected to the endoplasmic reticulum. J Cell Biol *182*, 685-701.

Buono, S., Ross, J.A., Tasfaout, H., Levy, Y., Kretz, C., Tayefeh, L., Matson, J., Guo, S., Kessler, P., Monia, B.P., *et al*. (2018). Reducing dynamin 2 (DNM2) rescues DNM2-related dominant centronuclear myopathy. Proc Natl Acad Sci U S A *115*, 11066-11071.

Catteruccia, M., Fattori, F., Codemo, V., Ruggiero, L., Maggi, L., Tasca, G., Fiorillo, C., Pane, M., Berardinelli, A., Verardo, M., *et al*. (2013). Centronuclear myopathy related to dynamin 2 mutations: clinical, morphological, muscle imaging and genetic features of an Italian cohort. Neuromuscul Disord *23*, 229-238.

Chino, H., Hatta, T., Natsume, T., and Mizushima, N. (2019). Intrinsically Disordered Protein TEX264 Mediates ER-phagy. Mol Cell.

Dooley, H.C., Razi, M., Polson, H.E., Girardin, S.E., Wilson, M.I., and Tooze, S.A. (2014). WIPI2 links LC3 conjugation with PI3P, autophagosome formation, and pathogen clearance by recruiting Atg12-5-16L1. Mol Cell *55*, 238-252.

Durieux, A.C., Vassilopoulos, S., Laine, J., Fraysse, B., Brinas, L., Prudhon, B., Castells, J., Freyssenet, D., Bonne, G., Guicheney, P., *et al*. (2012). A centronuclear myopathy--dynamin 2 mutation impairs autophagy in mice. Traffic *13*, 869-879.

Durieux, A.C., Vignaud, A., Prudhon, B., Viou, M.T., Beuvin, M., Vassilopoulos, S., Fraysse, B., Ferry, A., Laine, J., Romero, N.B., *et al*. (2010). A centronuclear myopathy-dynamin 2 mutation impairs skeletal muscle structure and function in mice. Hum Mol Genet *19*, 4820-4836.

Eskelinen, E.L. (2019). Autophagy: Supporting cellular and organismal homeostasis by self-eating. Int J Biochem Cell Biol *111*, 1-10.

Fass, E., Shvets, E., Degani, I., Hirschberg, K., and Elazar, Z. (2006). Microtubules support production of starvation-induced autophagosomes but not their targeting and fusion with lysosomes. J Biol Chem *281*, 36303-36316.

Ferguson, S.M., and De Camilli, P. (2012). Dynamin, a membrane-remodelling GTPase. Nat Rev Mol Cell Biol *13*, 75-88.

Gao, W., Chen, Z., Wang, W., and Stang, M.T. (2013). E1-like activating enzyme Atg7 is preferentially sequestered into p62 aggregates via its interaction with LC3-I. PLoS One *8*, e73229.

Hamasaki, M., Furuta, N., Matsuda, A., Nezu, A., Yamamoto, A., Fujita, N., Oomori, H., Noda, T., Haraguchi, T., Hiraoka, Y., *et al.* (2013). Autophagosomes form at ER-mitochondria contact sites. Nature *495*, 389-393.

Hansen, M., Rubinsztein, D.C., and Walker, D.W. (2018). Autophagy as a promoter of longevity: insights from model organisms. Nat Rev Mol Cell Biol *19*, 579-593.

Hayashi-Nishino, M., Fujita, N., Noda, T., Yamaguchi, A., Yoshimori, T., and Yamamoto, A. (2009). A subdomain of the endoplasmic reticulum forms a cradle for autophagosome formation. Nat Cell Biol *11*, 1433-1437.

Hohendahl, A., Roux, A., and Galli, V. (2016). Structural insights into the centronuclear myopathy-associated functions of BIN1 and dynamin 2. J Struct Biol *196*, 37-47.

Izumi, H., Li, Y., Shibaki, M., Mori, D., Yasunami, M., Sato, S., Matsunaga, H., Mae, T., Kodama, K., Kamijo, T., *et al.* (2019). Recycling endosomal CD133 functions as an inhibitor of autophagy at the pericentrosomal region. Sci Rep *9*, 2236.

Jacomin, A.C., Samavedam, S., Promponas, V., and Nezis, I.P. (2016). iLIR database: A web resource for LIR motif-containing proteins in eukaryotes. Autophagy *12*, 1945-1953.

Kabeya, Y., Mizushima, N., Ueno, T., Yamamoto, A., Kirisako, T., Noda, T., Kominami, E., Ohsumi, Y., and Yoshimori, T. (2000). LC3, a mammalian homologue of yeast Apg8p, is localized in autophagosome membranes after processing. EMBO J *19*, 5720-5728.

Kimura, S., Noda, T., and Yoshimori, T. (2007). Dissection of the autophagosome maturation process by a novel reporter protein, tandem fluorescent-tagged LC3. Autophagy *3*, 452-460.

Knaevelsrud, H., Carlsson, S.R., and Simonsen, A. (2013a). SNX18 tubulates recycling endosomes for autophagosome biogenesis. Autophagy *9*, 1639-1641.

Knaevelsrud, H., Soreng, K., Raiborg, C., Haberg, K., Rasmuson, F., Brech, A., Liestol, K., Rusten, T.E., Stenmark, H., Neufeld, T.P., *et al*. (2013b). Membrane remodeling by the PX-BAR protein SNX18 promotes autophagosome formation. J Cell Biol *202*, 331-349.

Longatti, A., Lamb, C.A., Razi, M., Yoshimura, S., Barr, F.A., and Tooze, S.A. (2012). TBC1D14 regulates autophagosome formation via Rab11- and ULK1-positive recycling endosomes. J Cell Biol *197*, 659-675.

Masiero, E., Agatea, L., Mammucari, C., Blaauw, B., Loro, E., Komatsu, M., Metzger, D., Reggiani, C., Schiaffino, S., and Sandri, M. (2009). Autophagy is required to maintain muscle mass. Cell Metab *10*, 507-515.

Menzies, F.M., Fleming, A., Caricasole, A., Bento, C.F., Andrews, S.P., Ashkenazi, A., Fullgrabe, J., Jackson, A., Jimenez Sanchez, M., Karabiyik, C., *et al*. (2017). Autophagy and Neurodegeneration: Pathogenic Mechanisms and Therapeutic Opportunities. Neuron *93*, 1015-1034.

Narain, Y., Wyttenbach, A., Rankin, J., Furlong, R.A., and Rubinsztein, D.C. (1999). A molecular investigation of true dominance in Huntington's disease. J Med Genet *36*, 739-746.

Peden, A.A., Schonteich, E., Chun, J., Junutula, J.R., Scheller, R.H., and Prekeris, R. (2004). The RCP-Rab11 complex regulates endocytic protein sorting. Mol Biol Cell *15*, 3530-3541.

Puri, C., Renna, M., Bento, C.F., Moreau, K., and Rubinsztein, D.C. (2013). Diverse autophagosome membrane sources coalesce in recycling endosomes. Cell *154*, 1285-1299.

Puri, C., Vicinanza, M., Ashkenazi, A., Gratian, M.J., Zhang, Q., Bento, C.F., Renna, M., Menzies, F.M., and Rubinsztein, D.C. (2018a). The RAB11A-Positive Compartment Is a Primary Platform for Autophagosome Assembly Mediated by WIPI2 Recognition of PI3P-RAB11A. Dev Cell *45*, 114-131 e118.

Puri, C., Vicinanza, M., and Rubinsztein, D.C. (2018b). Phagophores evolve from recycling endosomes. Autophagy *14*, 1475-1477.

Ravikumar, B., Moreau, K., Jahreiss, L., Puri, C., and Rubinsztein, D.C. (2010). Plasma membrane contributes to the formation of pre-autophagosomal structures. Nat Cell Biol *12*, 747-757.

Ross, J.A., Digman, M.A., Wang, L., Gratton, E., Albanesi, J.P., and Jameson, D.M. (2011). Oligomerization state of dynamin 2 in cell membranes using TIRF and number and brightness analysis. Biophys J *100*, L15-L17.

Shibutani, S.T., and Yoshimori, T. (2014). A current perspective of autophagosome biogenesis. Cell Res *24*, 58-68.

Soreng, K., Munson, M.J., Lamb, C.A., Bjorndal, G.T., Pankiv, S., Carlsson, S.R., Tooze, S.A., and Simonsen, A. (2018). SNX18 regulates ATG9A trafficking from recycling endosomes by recruiting Dynamin-2. EMBO Rep *19*.

Sundborger, A.C., and Hinshaw, J.E. (2014). Regulating dynamin dynamics during endocytosis. F1000Prime Rep *6*, 85.

Takahashi, Y., He, H., Tang, Z., Hattori, T., Liu, Y., Young, M.M., Serfass, J.M., Chen, L., Gebru, M., Chen, C., *et al*. (2018). An autophagy assay reveals the ESCRT-III component CHMP2A as a regulator of phagophore closure. Nat Commun *9*, 2855.

Tang, D., Kang, R., Berghe, T.V., Vandenabeele, P., and Kroemer, G. (2019). The molecular machinery of regulated cell death. Cell Res *29*, 347-364.

Trochet, D., Prudhon, B., Beuvin, M., Peccate, C., Lorain, S., Julien, L., Benkhelifa-Ziyyat, S., Rabai, A., Mamchaoui, K., Ferry, A., *et al*. (2018). Allele-specific silencing therapy for Dynamin 2-related dominant centronuclear myopathy. EMBO Mol Med *10*, 239-253.

Tung, Y.T., Hsu, W.M., Lee, H., Huang, W.P., and Liao, Y.F. (2010). The evolutionarily conserved interaction between LC3 and p62 selectively mediates autophagy-dependent degradation of mutant huntingtin. Cell Mol Neurobiol *30*, 795-806.

van Dam, E.M., and Stoorvogel, W. (2002). Dynamin-dependent transferrin receptor recycling by endosome-derived clathrin-coated vesicles. Mol Biol Cell *13*, 169-182.

Vicinanza, M., Korolchuk, V.I., Ashkenazi, A., Puri, C., Menzies, F.M., Clarke, J.H., and Rubinsztein, D.C. (2015). PI(5)P regulates autophagosome biogenesis. Mol Cell *57*, 219-234.

Yin, Z., Pascual, C., and Klionsky, D.J. (2016). Autophagy: machinery and regulation. Microb Cell *3*, 588-596.

Yla-Anttila, P., Vihinen, H., Jokitalo, E., and Eskelinen, E.L. (2009). 3D tomography reveals connections between the phagophore and endoplasmic reticulum. Autophagy *5*, 1180-1185.

Yoshii, S.R., Kuma, A., Akashi, T., Hara, T., Yamamoto, A., Kurikawa, Y., Itakura, E., Tsukamoto, S., Shitara, H., Eishi, Y., *et al*. (2016). Systemic Analysis of Atg5-Null Mice Rescued from Neonatal Lethality by Transgenic ATG5 Expression in Neurons. Dev Cell *39*, 116-130.

Zhao, M., Maani, N., and Dowling, J.J. (2018). Dynamin 2 (DNM2) as Cause of, and Modifier for, Human Neuromuscular Disease. Neurotherapeutics *15*, 966-975.

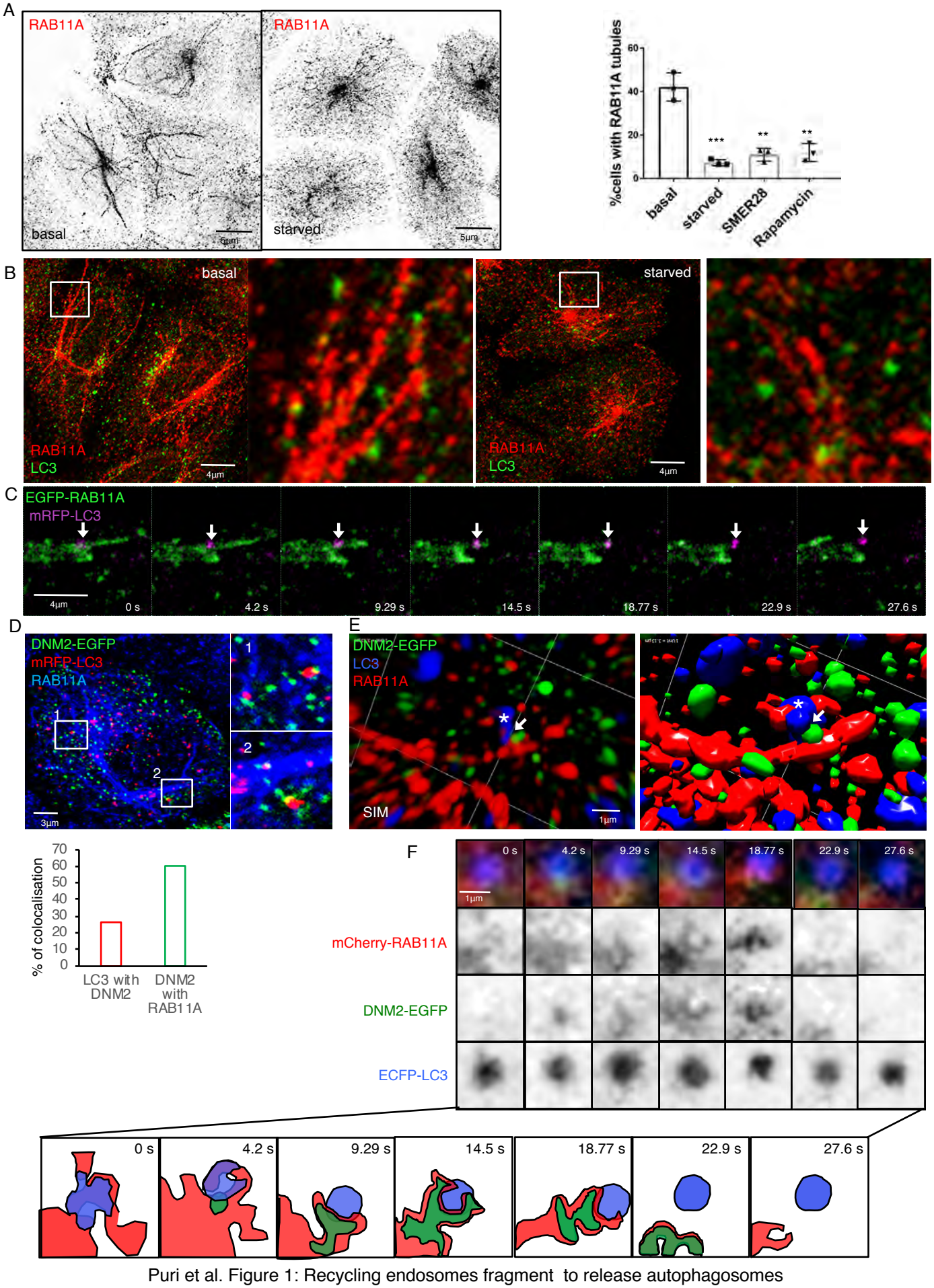

Puri et al. Figure 1: Recycling endosomes fragment to release autophagosomes

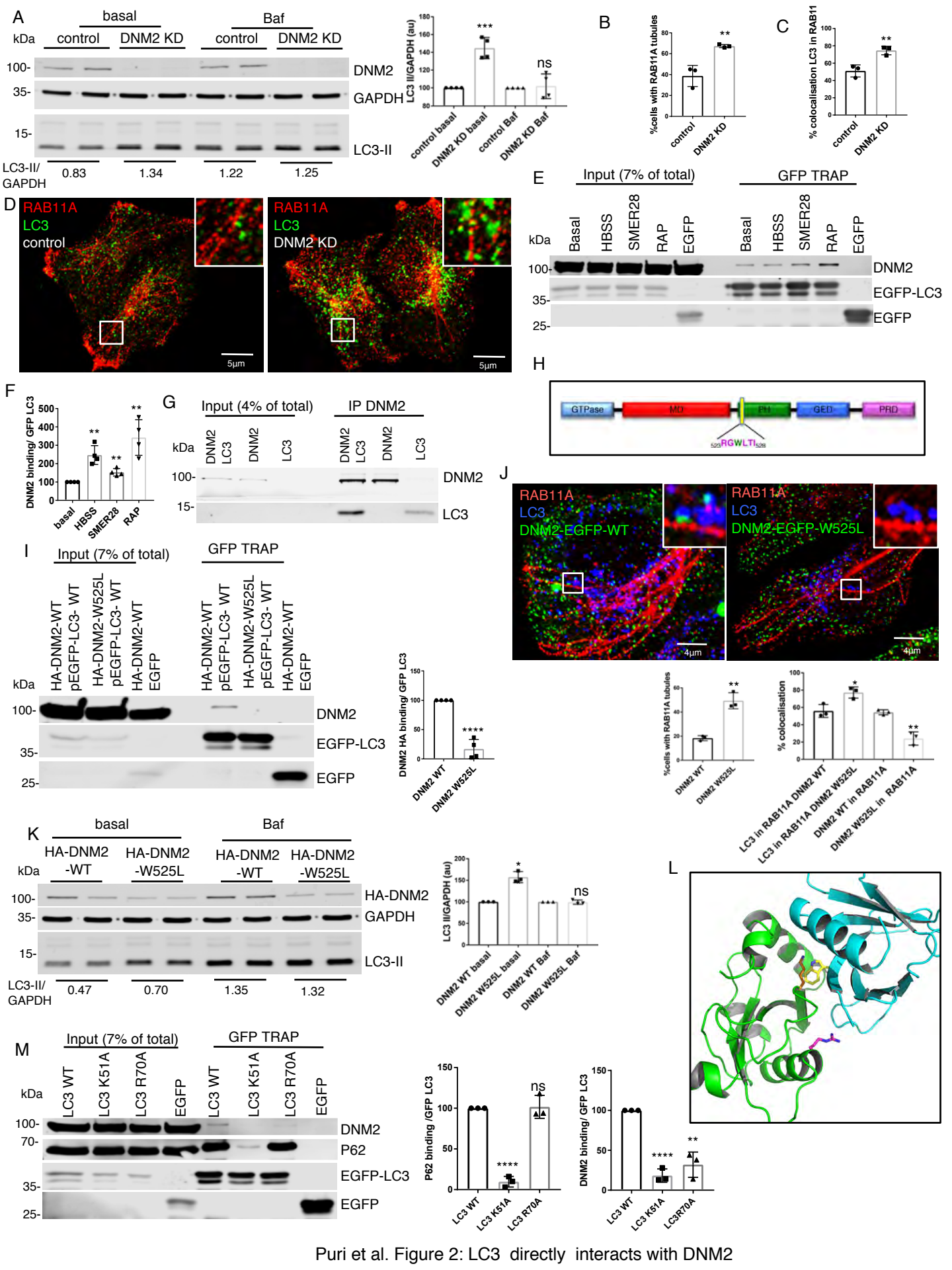

Puri et al. Figure 2: LC3 directly interacts with DNM2

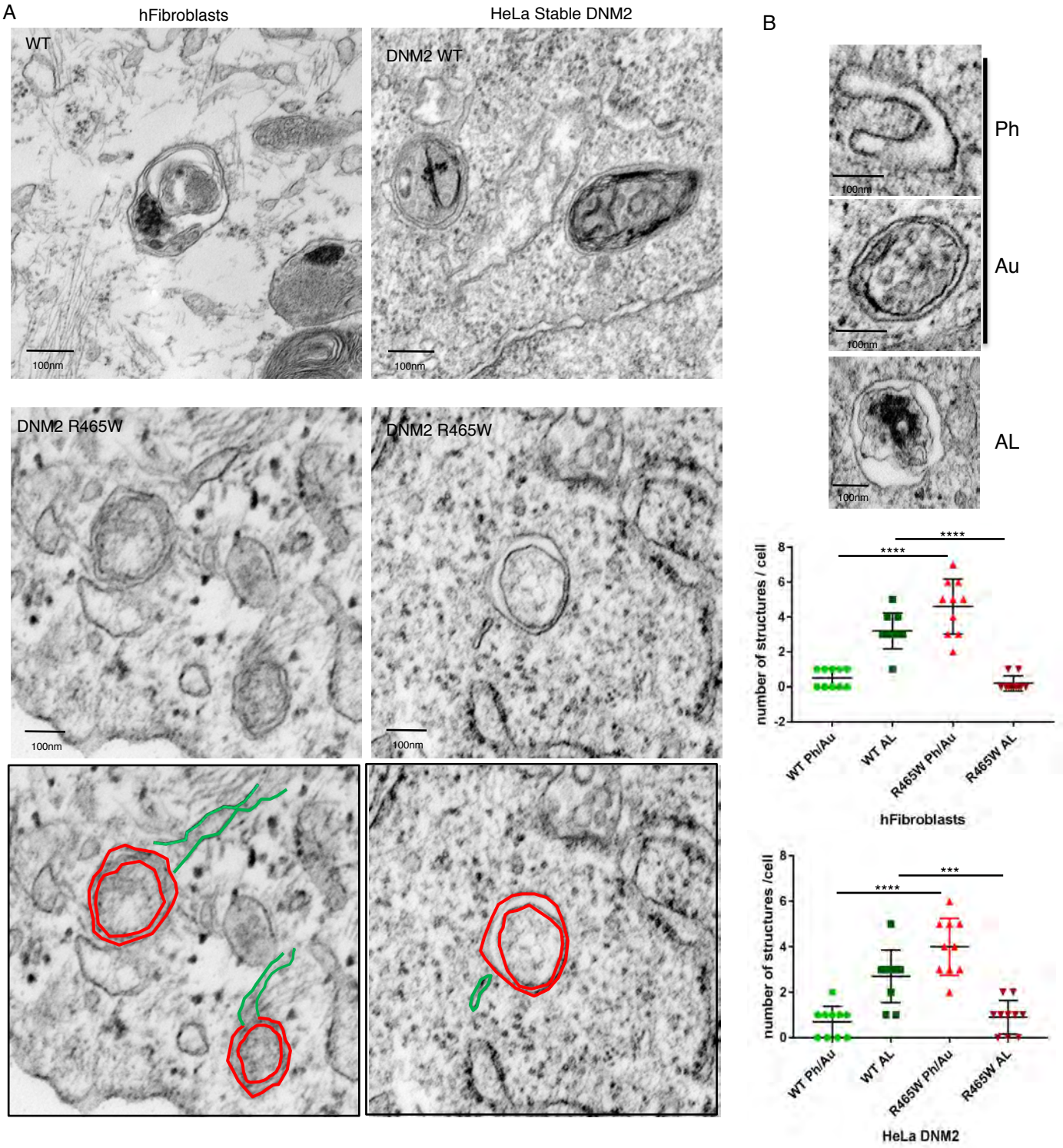

Puri et al. Figure 3: DNM2 R465W accumulates immature autophagosomes

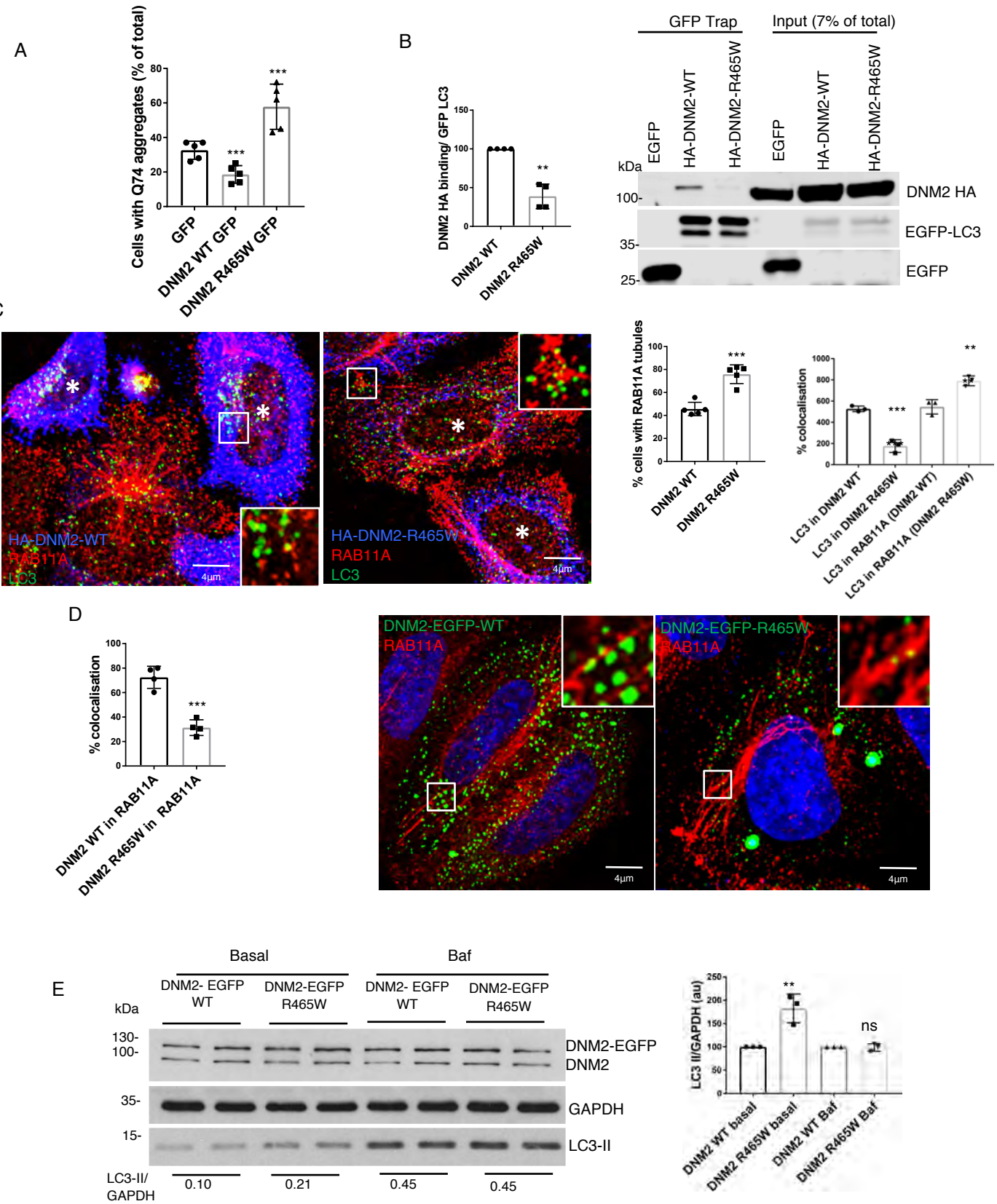

Puri et al. Figure 4: DNM2 R465W accumulates autophagosomes on recycling endosomes

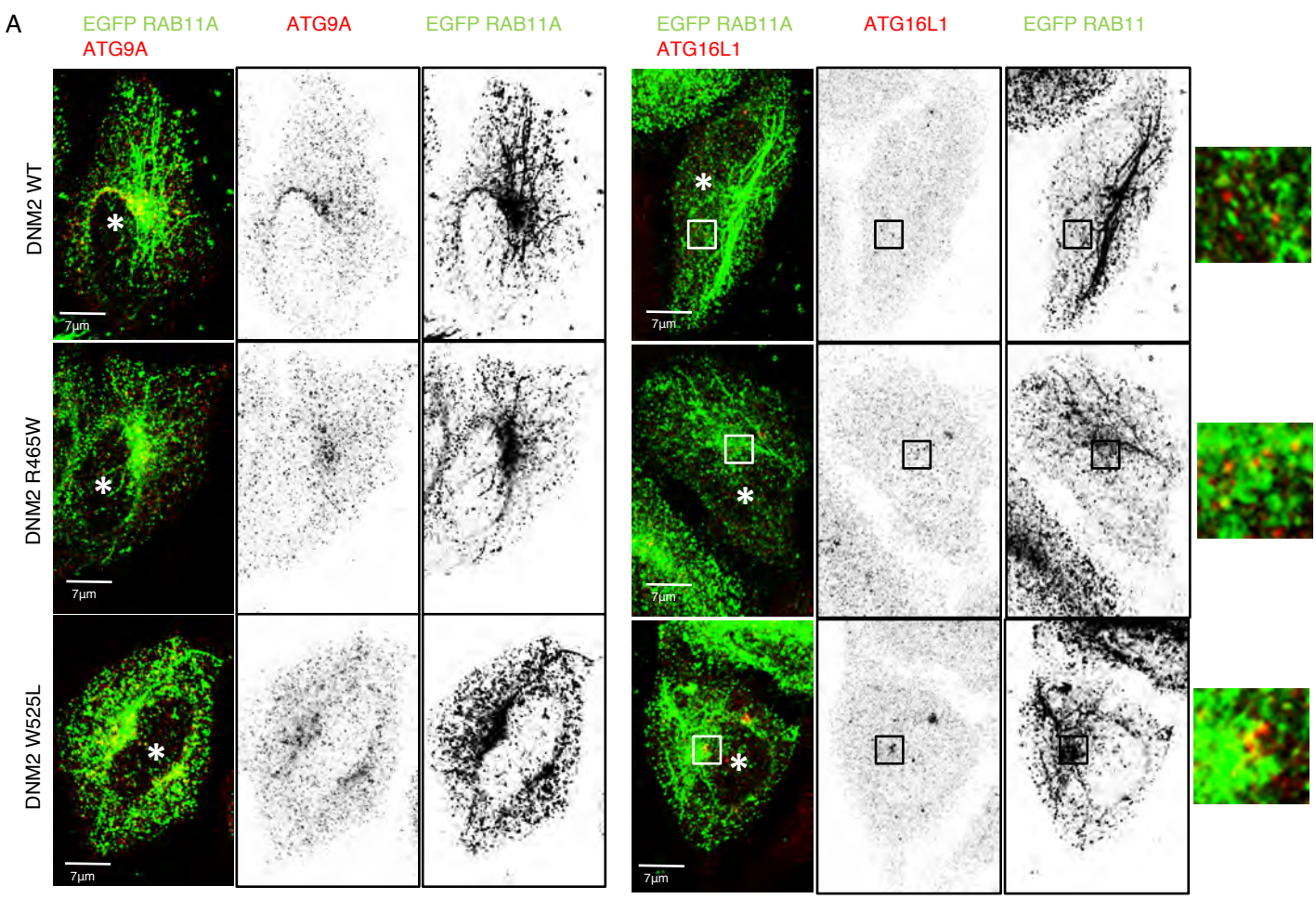

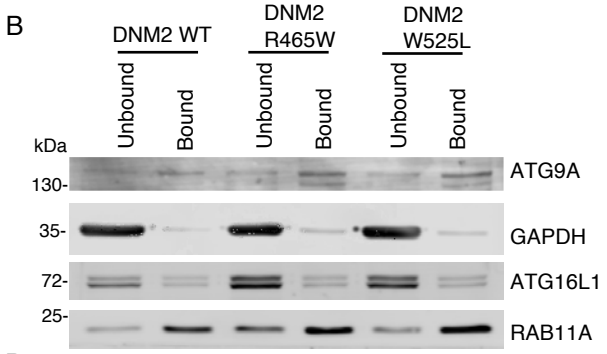

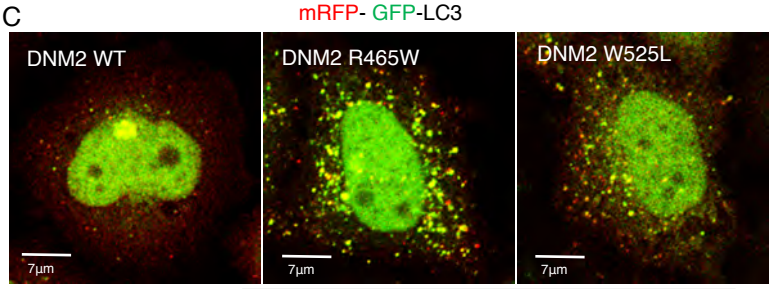

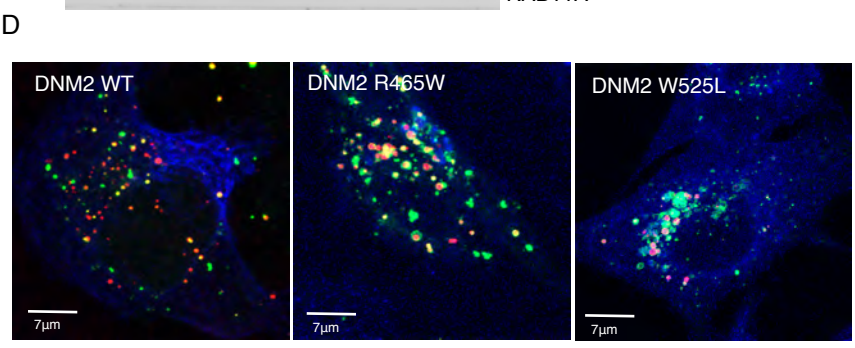

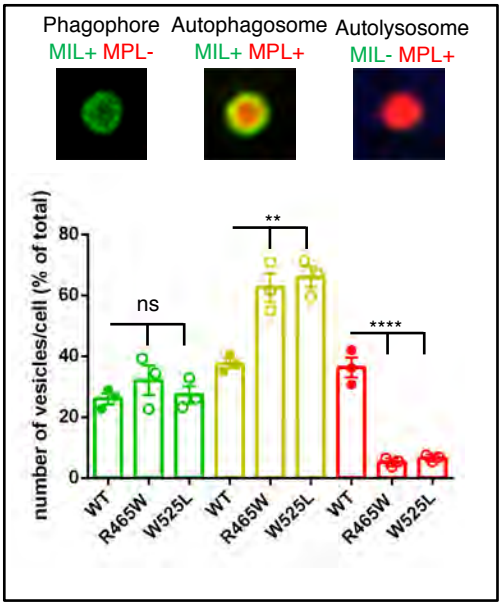

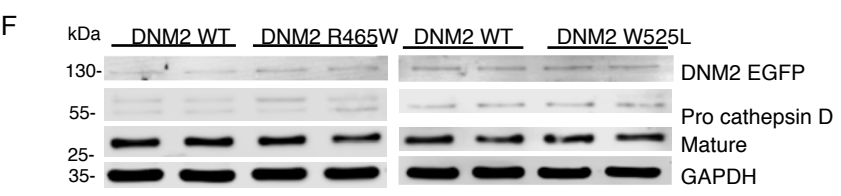

Puri et al. Figure 5: DNM2 mutants accumulates immature autophagosomes

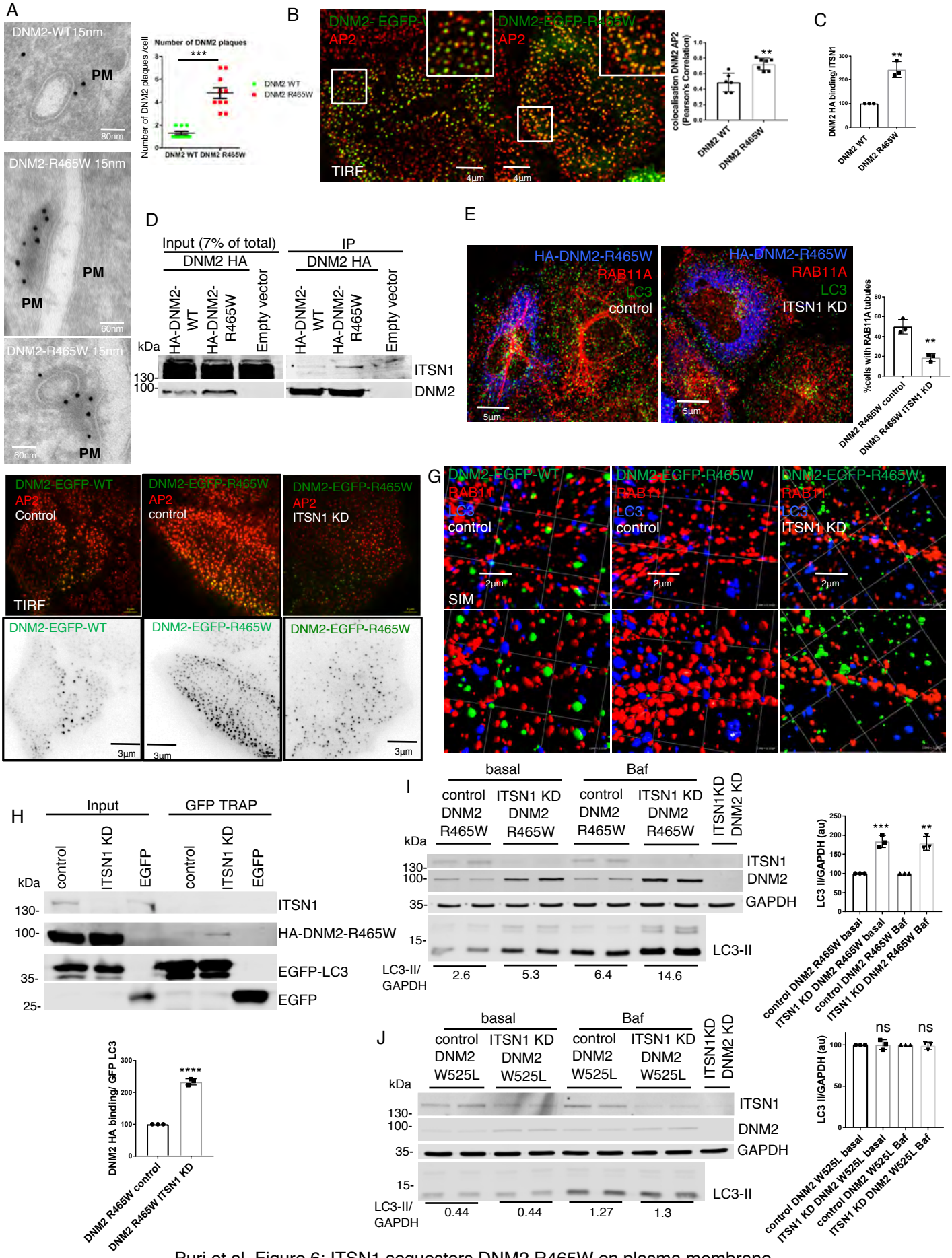

Puri et al. Figure 6: ITSN1 sequesters DNM2 R465W on plasma membrane

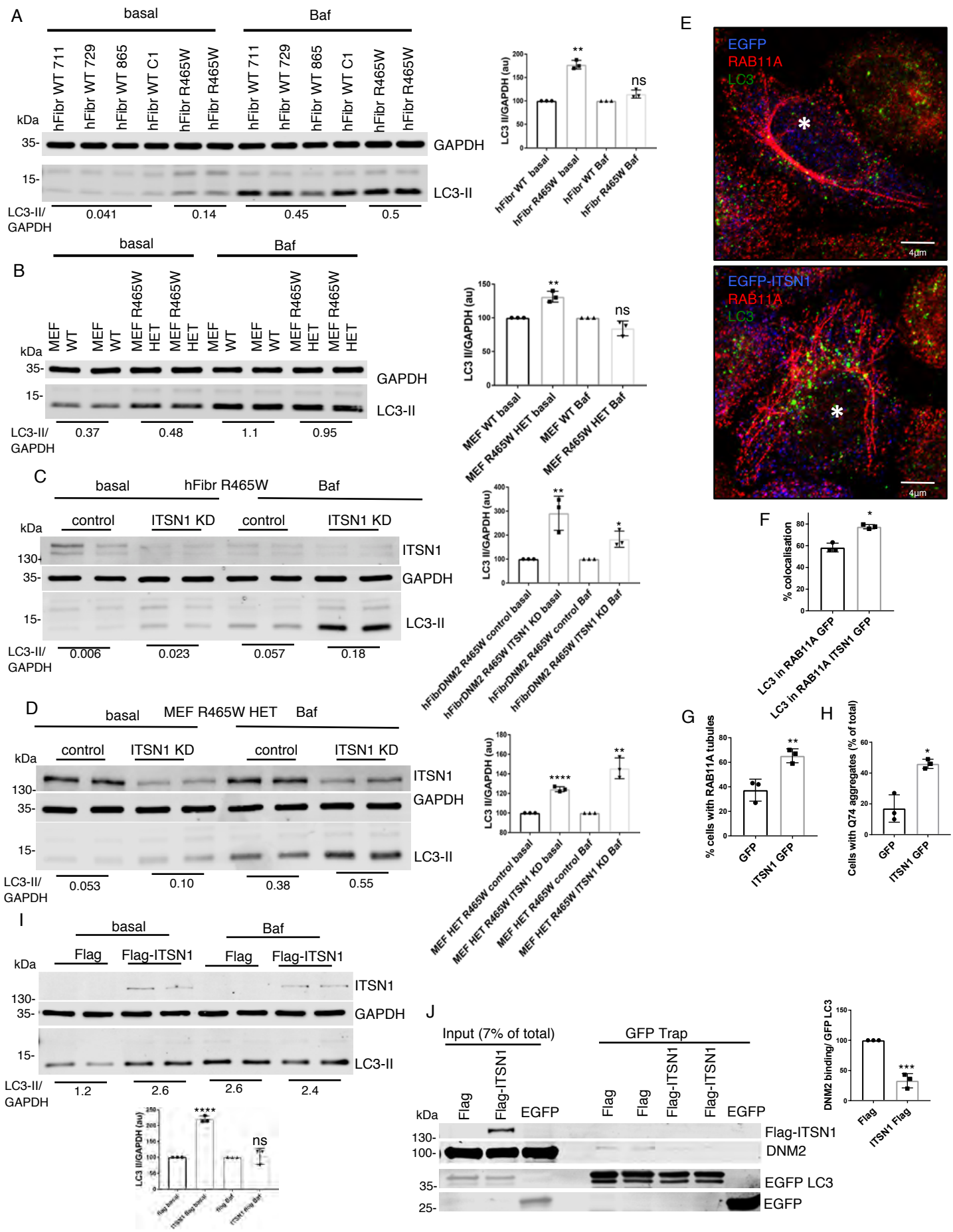

Puri et al. Figure 7: R465W Fibroblasts confirm the phenotype observed in HeLa and overexpression of ITSN1 mimics the phenotype

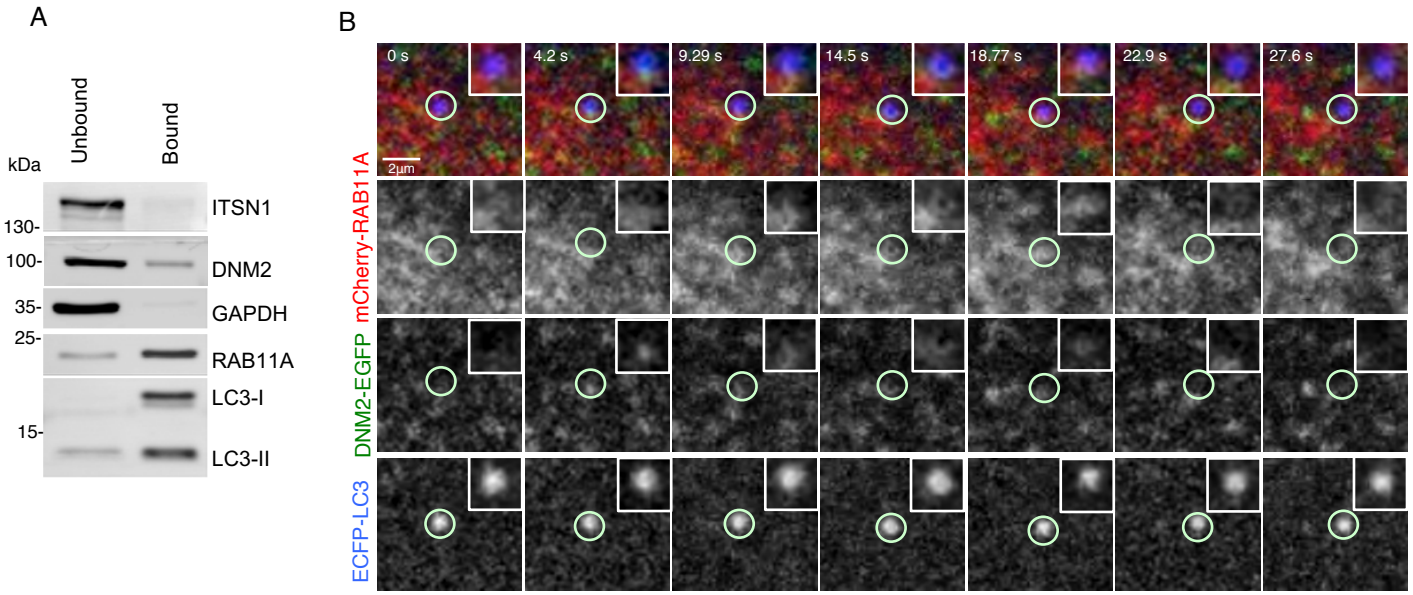

Puri et al. Figure S1 (related to Figure 1): Recycling endosomes fragment to release autophagosomes

Figure S1 (related to Figure 1):Recycling endosomes fragment to release autophagosomes

A) HeLa cells were starved 1 h in HBSS, loaded with Ferrofluid-Tf Alexa488 for 1 h in HBSS and chased for 15 min in HBSS. The cells were then fragmented and the membranes containing Ferrofluid-Tf488 (B=bound) or not containing Ferrofluid-Tf488 (U=unbound) were separated, lysed and processed for immunoblotting as indicated (see technical details in Material and Methods).

B) HeLa cells were transfected for 24 h with mCherry-RAB11A, DNM2-pEGFP and pECFP-LC3 and processed for live imaging in HEPES-HBSS medium (See also Fig. 1F Movie 2).

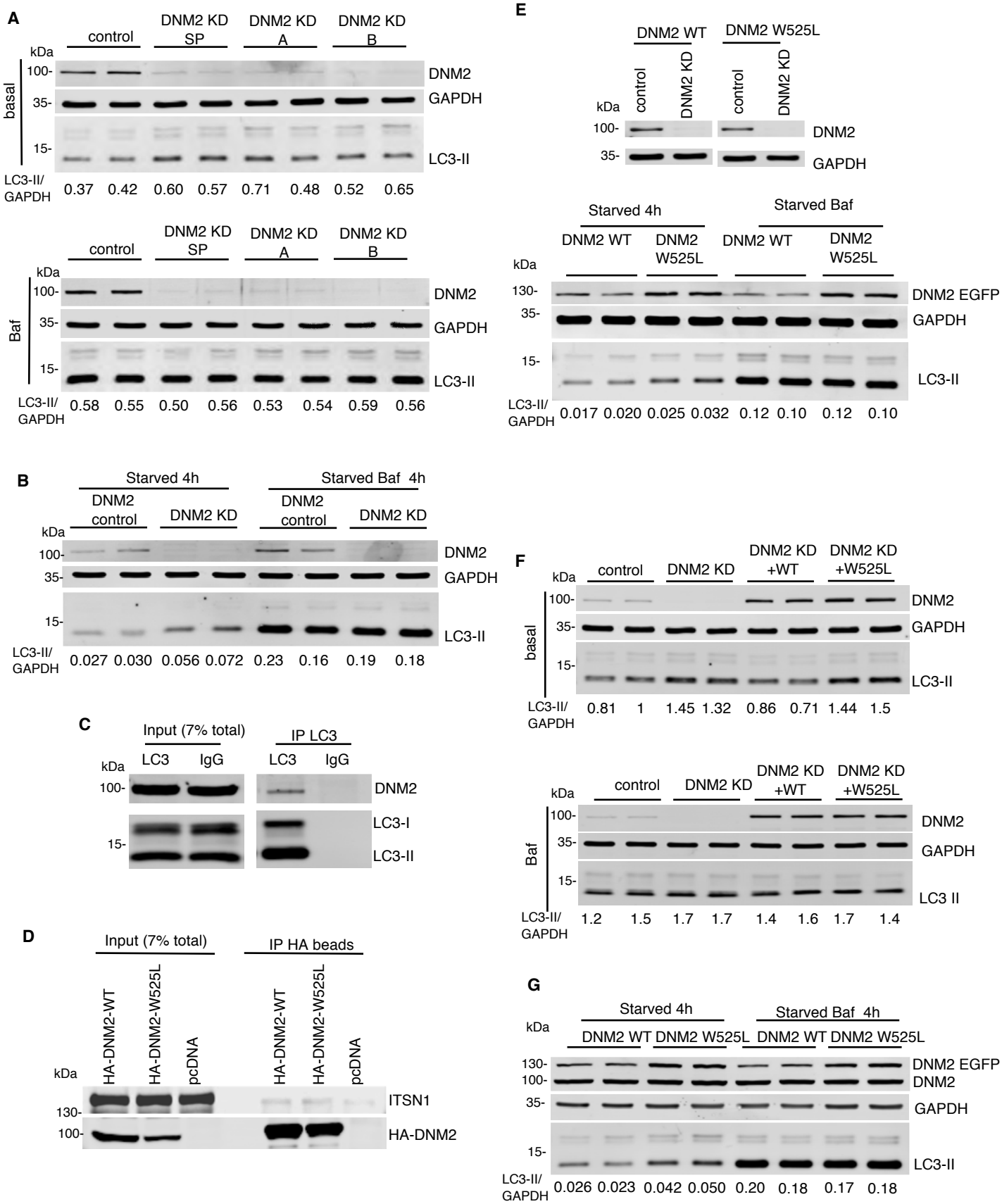

Puri et al. Figure S2 (related to Figure 2): DNM2 KD and LIR mutant (W525L) accumulates autophagosomes

Figure S2 (related to Figure 2): DNM2 KD and LIR mutant (W525L) accumulates autophagosomes

A) HeLa cells transfected with DNM2 siRNA Smart Pool oligos (SP), or oligo A or oligo B for 3 days were treated with DMSO (basal) or Bafilomycin A1 (Baf) for 4 h, processed for immunoblot and labeled LC3, DNM2 and GAPDH as loading control. The numbers below indicate the LC3-II/GAPDH values of the representative blot (one representative experiment of two).

B) HeLa cells transfected with DNM2 siRNA (mix of oligos A and B) for 3 days were starved (HBSS with DMSO) (Starved 4 h) or with HBSS/Bafilomycin A1 (Starved Baf 4 h) for 4 h, processed for immunoblot and labeled LC3, DNM2 and GAPDH as loading control. The numbers below indicate the LC3-II/GAPDH values of the representative blot (one representative experiment of two).

C) HeLa cells in basal condition were lysed and immunoprecipitated with anti-LC3 antibody or with negative control antibody and blotted for DNM2 and LC3.

D) HeLa cells transfected with DNM2 siRNA oligos (mix of oligos A and B) for 3 days and transfected for the last 20 h with HA-DNM2-WT or W525L or empty vector. Immunoprecipitates obtained by HA-conjugated magnetic beads (Pierce™ Anti-HA Magnetic Beads- 88836), were processed for immunoblot for HA-DNM2 and ITSN1.

E) HeLa cells stably expressing DNM2-pEGFP- WT or W525L transfected with DNM2 siRNA (mix of oligos A and B) for 3 days were starved (HBSS with DMSO) (Starved 4 h) or with HBSS/Bafilomycin A1 (Starved Baf 4 h) for 4 h, processed for immunoblot and labeled LC3, DNM2 and GAPDH as loading control. The Western blot above shows the level of DNM2 endogenous KD. The numbers below indicate the LC3-II/GAPDH value of the representative experiment (one representative experiment of two).

F) HeLa cells transfected with DNM2 siRNA oligos (mix of oligos A and B) or control oligos for 3 days, were subsequently transfected for the last 20 h with HA-DNM2-WT or W525L, or not. Lysates were treated with DMSO (basal) or Bafilomycin A1 (Baf) for 4 h and processed for immunoblot and labeled LC3, DNM2 and GAPDH as loading control. The numbers below indicate the LC3-II/GAPDH value of the experiment.

G) HeLa cells stably expressing DNM2-pEGFP-WT or W525L were starved (HBSS with DMSO) (Starved 4 h) or with HBSS/Bafilomycin A1 (Starved Baf 4h) for 4 h, processed for immunoblot and labeled LC3, DNM2 and GAPDH as loading control. The numbers below indicate the LC3-II/GAPDH value of the representative experiment (one representative experiment of two).

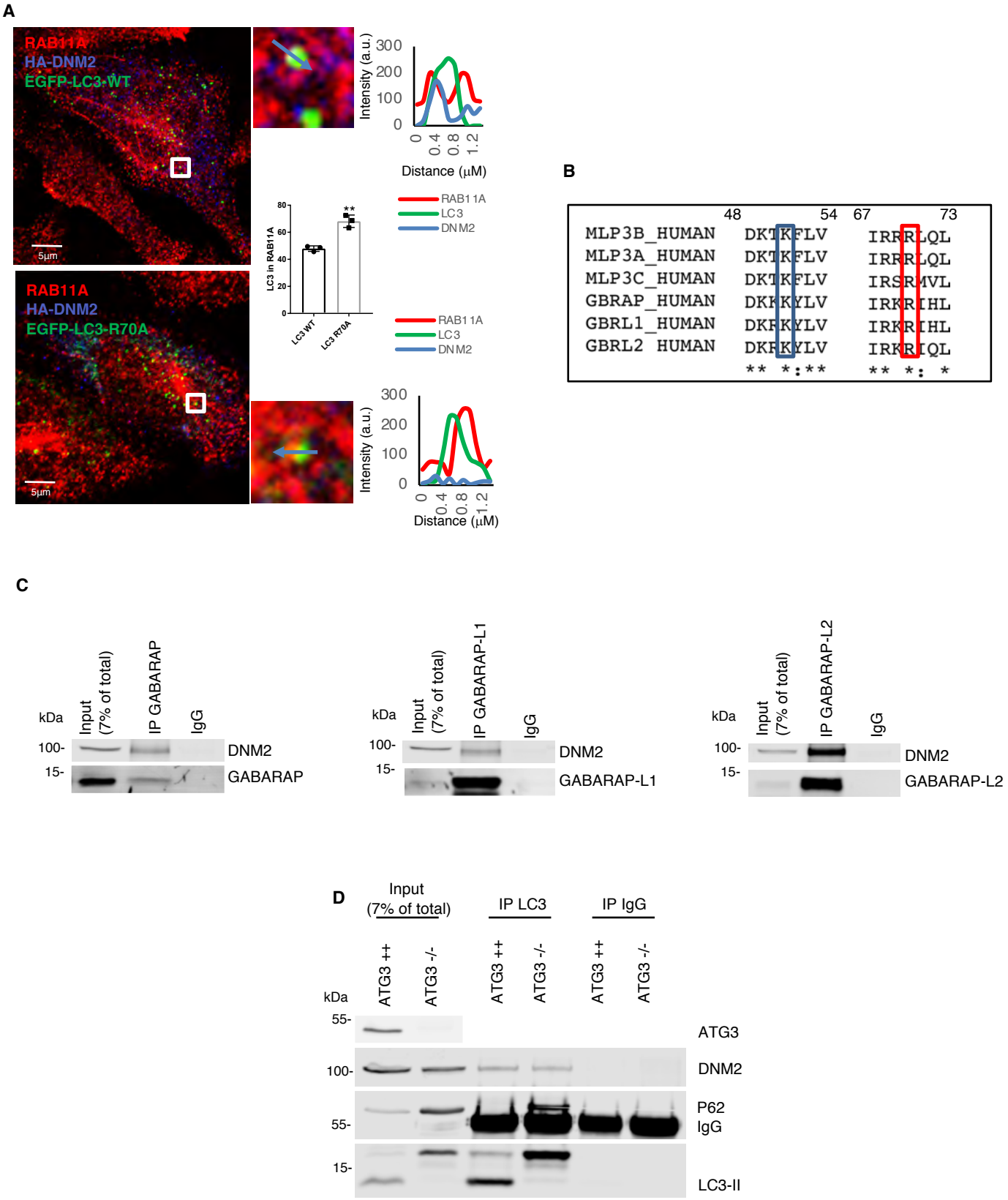

Puri et al. Figure S3 (related to Figure 2) : LC3-DNM2 binding motive is conserved on ATG8 family member

Figure S3 (related to Figure 2): LC3-DNM2 binding motive is conserved on ATG8 family member

A) HeLa cells were transfected with pEGFP-LC3-WT or R70A and HA-DNM2-WT for 20 h, fixed and labelled for endogenous RAB11A and anti-HA. Histogram shows the quantification of the association of LC3 with RAB11A (Manders' Coefficient). Data are mean ± SD (n=3; graphs represent means of the triplicates from three independent experiments). Two-tailed paired t test, **=$p<0.01$. Line scan analysis of selected areas is shown.

B) Alignment of ATG8 family members using UniProt showing conserved K and R residues corresponding to K51 and R70 in LC3B. * are residues that are completely conserved and **:** are partially conserved residues.

C) HeLa cells in basal condition were lysed and immunoprecipitated with anti-GABARAP, anti-GABARAP L1, anti-GABARAP L2 antibody or with negative control antibody and blotted for DNM2 and GABARAP, GABARAP L1, GABARAP L2.

D) HeLa-Cas9 or ATG3-knockout (KO) CRISPR-Cas9 cells in basal condition were lysed and immunoprecipitated with anti-LC3 antibody or with negative control antibody and blotted for DNM2, LC3 and P62.

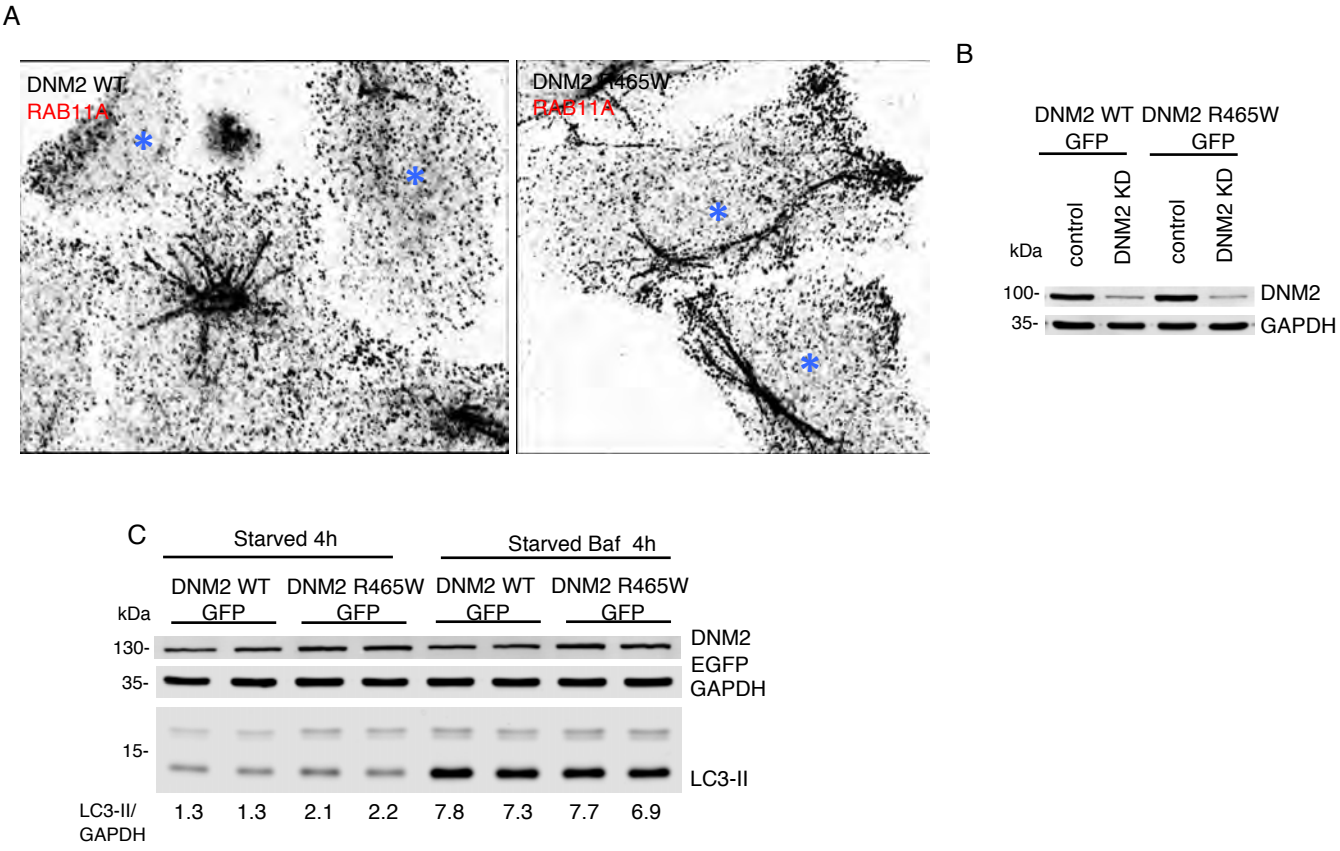

Puri et al. Figure S4 (related to Figure 4): DNM2 R465W accumulates autophagosomes on recycling endosomes

Figure S4 (related to Figure 4): DNM2 R465W accumulates autophagosomes on recycling endosomes

A) HeLa cells were transfected for 20 h with HA-DNM2-WT or R465W. Red channel only (RAB11A labelling) of the pictures in 4C.

B-C) HeLa cells stably expressing DNM2-pEGFP- WT or R465W transfected with DNM2 siRNA (mix of oligos A and B) for 3 days were starved (HBSS with DMSO) (Starved 4 h) or with HBSS/Bafilomycin A1 (Starved Baf 4 h) for 4 h, processed for immunoblot and labeled LC3, DNM2 and GAPDH as loading control. The Western blot in B shows the level of DNM2 endogenous KD. The numbers below indicate the LC3-II/GAPDH value of the representative experiment (one representative experiment of two).

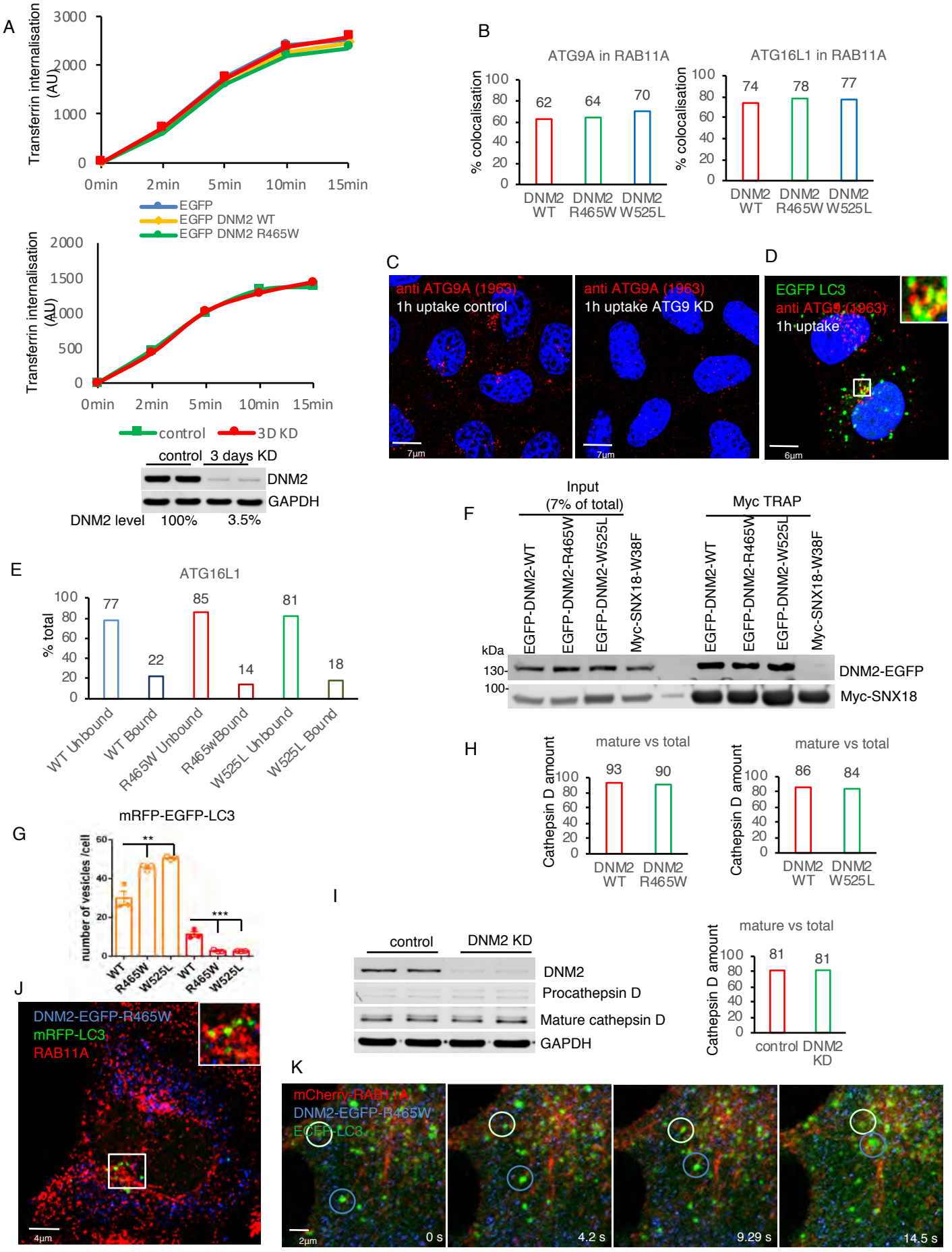

Puri et al. Figure S5 (related to Figure 5): DNM2 mutants accumulates immature autophagosomes

Figure S5 (related to Figure 5): DNM2 mutants accumulates immature autophagosomes

A) HeLa cells transfected for 20 h with pEGFP empty vector or DNM2-pEGFP-WT or R465W or W525L were loaded with transferrin Alexa-647 for different times (0, 2, 5, 10 and 15 minutes). The amount of transferrin internalized in cells expressing EGFP was measured by Flow Cytometry Analysis (FACS). Alternatively, HeLa cells transfected with control siRNA or DNM2 oligos (mix of oligos A and B) for 3 days and treated as described above. The blot below shows the amount of DNM2 that is left after three days knockdown (3.5% of control).

B) Histogram shows the quantification of the association of ATG9A or ATG16L1 with RAB11A (Manders' Coefficient) of the images shown in Fig. 5A.

C) HeLa cells transfected with control or ATG9A siRNA oligos for 5 days, and loaded with antibody (1963) anti-ATG9A II extracellular loop in starving condition (HBSS) for 1 h and processed for immunofluorescence.

D) HeLa cells transfected for 20 h with pEGFP-LC3 and treated as described in C. The insert show shows the vesicles containing both ATG9A and EGFP-LC3.

E) HeLa cells stably expressing DNM2 -pEGFP WT, DNM2 -pEGFP R465W or DNM2 -pEGFP W525L were starved for 1 h in HBSS, loaded with Ferrofluid-anti-ATG9A antibody for 1 h in HBSS and chased for 15 min in HBSS. The cells were then fragmented and the membranes containing Ferrofluid-anti-ATG9 (Bound) or not containing Ferrofluid-anti-ATG9 (Unbound) were separated, lysed and processed for immunoblotting as indicated (see technical details in Material and Methods). The histogram shows the quantification of ATG16L1 amount in the unbound or bound fractions in the different cell lines.

F) HeLa cells transfected for 20 h with DNM2-pEGFP-WT or R465W or W525L in combination with Myc-SNX18-WT and processed for Myc-TRAP. Cells transfected with DNM2-pEGFP-WT and Myc-SNX18-W38F mutant were used as negative control.

G) HeLa stable cell line stable expressing the tandem-tagged mRFP-GFP-LC3 were transfected for 20 h with HA-DNM2 WT or HA-DNM2 R465W or HA DNM2-W525L and labelled with anti-HA to visualize the transfected cells. The histogram shows the quantification of the experiment shown in Fig. 5C. The orange bars represent the numbers of yellow (red and green) unacidified autophagosomes and the red bars represent the red-only, acidified autophagosomes/autolysosomes. Data are mean ± SD (n=3, graphs represent means of the triplicates from three independent experiments). Two-tailed paired t test, **=$p<0.01$, ***= $p<0.001$.

H) The histogram shows the quantification of the experiment shown in Fig. 5F.

I) HeLa cells transfected with DNM2 control siRNA or DNM2 oligos (mix of oligos A and B) for 3 days and were processed for western blot to analyze the amount of pro- or mature Cathepsin D. The ratio of mature vs total Cathepsin D were analyzed and the results are shown in the histogram on the right.

J) HeLa cells transfected for 20 h with DNM2-pEGFP-R465W and mRFP-LC3 were labelled for endogenous RAB11A.

K) HeLa cells were transfected for 24 h with mCherry-RAB11A, DNM2-pEGFP-R465W and pECFP-LC3 and processed for live imaging in HEPES-HBSS medium (See also Movie 3).

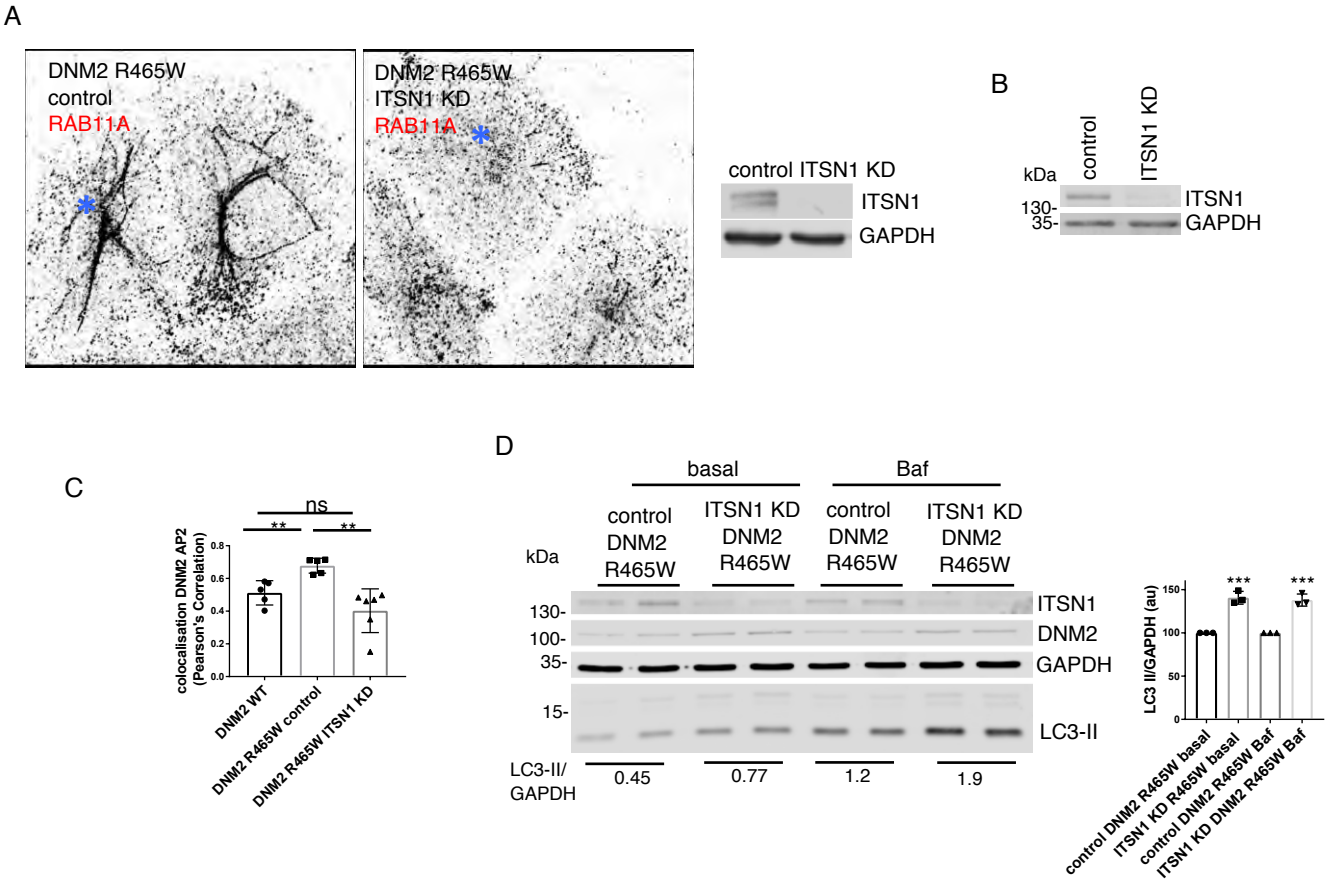

Puri et al. Figure S6 (related to Figure 6): ITSN1 sequesters DNM2 R465W on plasma membrane

Figure S6 (related to Figure 6): ITSN1 sequesters DNM2 R465W on plasma membrane

A) HeLa cells transfected with control or ITSN1 siRNA oligos for 3 days were transfected for 20 h with HA-DNM2-R465W. Red channel only (RAB11A labelling) of the pictures in 6E and the relative level of ITSN1 knockdown (KD).

B-C) HeLa cells were transfected with pEGFP-empty or pEGFP-DNM2 -WT or R465W for 24 h, fixed and labelled for endogenous AP2 and processed for Total Internal Reflection Fluorescence (TIRF). The blot in B shows the level of ITSN1 KD. The histogram in C shows the quantification of the association of DNM2 with AP2 (Pearson's Correlation). Data are mean ± SD (n=5 cells each condition) two-tailed paired t-test, **=$p<0.01$.

D) HeLa cells transfected with control or ITSN1 siRNA oligos for 3 days and were transfected in the last 20 h with HA-DNM2-R465W. The cells were treated with DMSO (basal) or Bafilomycin A1 (Baf) for 4 h, processed for immunoblot and labeled for LC3, HA-DNM2 and GAPDH as loading control. The histogram shows the relative amount of LC3-II in basal or under Baf treatment normalized for GAPDH. Data are mean ± SD (n=3, graphs represent means of the triplicates from three independent experiments) two-tailed paired *t*-test, ***=$p<0.001$. The numbers below indicate the LC3-II/GAPDH value of the shown experiment.

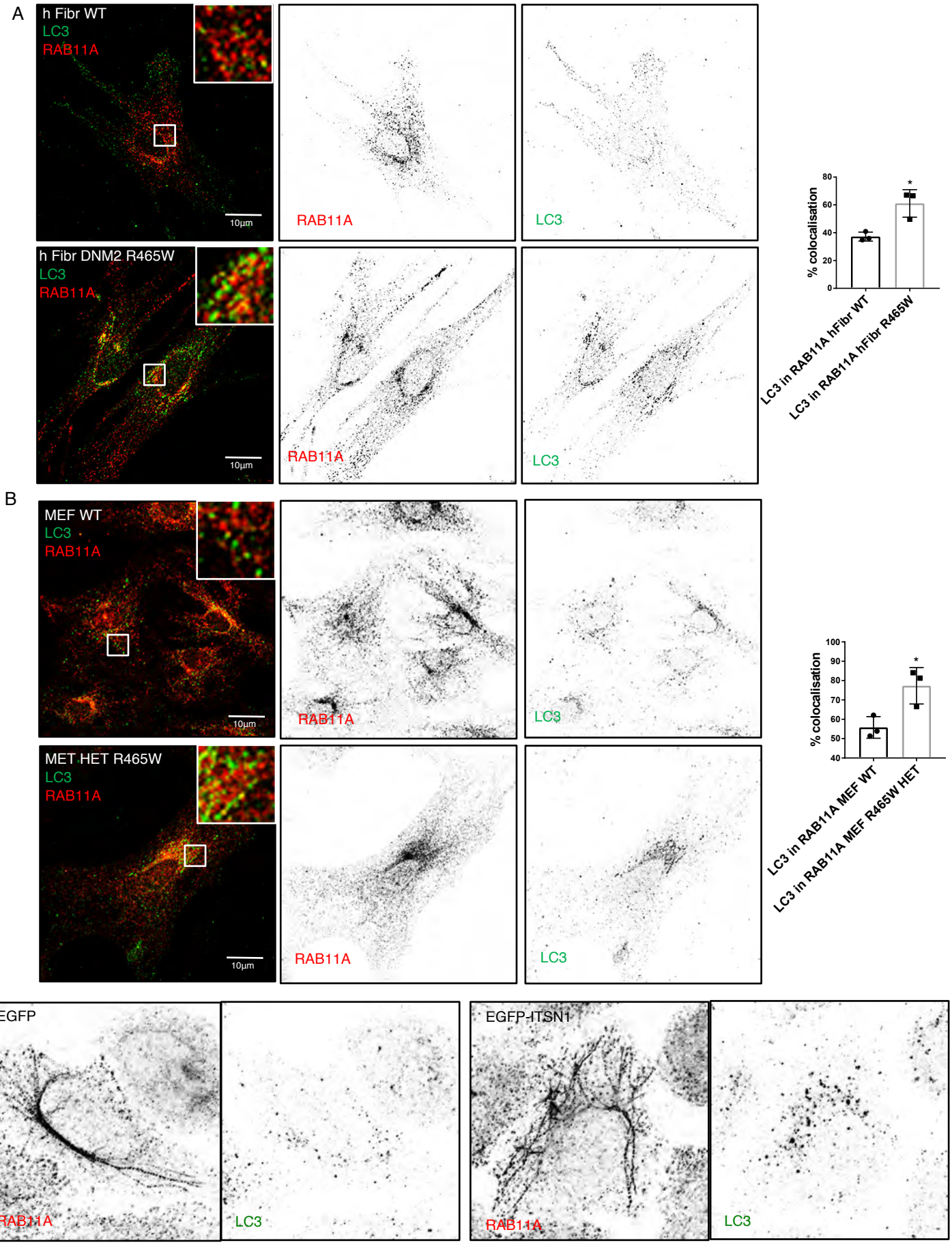

Puri et al. Figure S7 (related to Figure 7): R465W Fibroblasts confirm the phenotype observed in HeLa and overexpression of ITSN1 mimics the phenotype

Figure S7 (related to Figure 7): R465W Fibroblasts confirm the phenotype observed in HeLa and overexpression of ITSN1 mimics the phenotype

A-B) WT human fibroblasts and R465W mutant (from CNM patient) or WT or R465W HET MEF were fixed for immunofluorescence and labelled for endogenous LC3 and RAB11A. Histogram on the right shows the quantification of the association of LC3 with RAB11A (Manders' Coefficient). Data are mean ± SD (n=3, graphs represent means of the triplicates from three independent experiments). Two-tailed paired t test, *=$p<0.05$.

C) HeLa cells were transfected for 20 h with pEGFP-ITSN1 or pEGFP empty vector. The cells were fixed for endogenous LC3 and RAB11A. Red channel only (RAB11A labelling) of the pictures in 7E.